



Westinghouse Electric Corporation

A Westinghouse Division

National Aeronautics and Space Administration
George C. Marshall Space Flight Center
Huntsville, Alabama 35812

Attention: Mr. John R. Jones
Contracting Officer, PR-RC

Subject: Review of Interim Technical Progress
Contract NAS 8-11929, Phase I

MAY 11 1966

GPO PRICE \$ _____

CFSTI PRICE(S) \$ _____

Hard copy (HC) 3.00

Microfiche (MF) 1.75

if 653 July 65

Gentlemen:

Attached is one copy of an interim technical memo summarizing the findings of the subject program through April 15, 1966. This memo is not a contractual requirement but is being furnished to assist technical personnel in their evaluation of the program and in planning future applications of the equipment.

It is considered appropriate to make such a report at this time since many of the problems originally felt to be capable of placing constraints on the use of the subject equipment (particularly those relating to penetration and porosity) have been resolved. The equipment is now free to enter a project period which emphasizes the metallurgical potential of the process without concern for these original constraints.

Further distribution is being made this date in accordance with instructions given in your letter of September 17, 1965.

Respectfully,
ORIGINAL SIGNED BY
H. F. FAUGHT
H. F. Faught
Program Manager

/FDS

Enclosure - 1

cc: MS-IL, NASA-MSFC, w/2 enclosures
MS-T, NASA-MSFC, w/1 enclosure
R-ME-MW/H. Lienau, NASA-MSFC, w/6 enclosures

(THRU)
(CODE) 15
(CATEGORY)

N66. 389.17
(ACCESSION NUMBER)
89
(PAGES)
CR-78673
(NASA OR TX OR AD NUMBER)

RELATIONSHIPS BETWEEN WELD QUALITY
AND NON-VACUUM ELECTRON BEAM
WELDING PROCEDURES

TECHNICAL PROGRESS SUMMARY
June 15, 1965 through February 15, 1966
NAS 8-11929 PHASE I

F. D. Seaman

Westinghouse Electric Corporation
Astronuclear Laboratory

ABSTRACT

Critical procedure details for non-vacuum electron beam welds have been identified and related to such qualities as undercut, bead width, contour and porosity. Welds that are consistent with actual quality standards have been produced. The strength of one-side welds produced at 3.6 KW power (approximately 28 Kilojoules-heat input/unit length per unit thickness) followed the heat input strength relationship and were equivalent to GTA welds. Welds of similar cross section but produced at lower unit heat input levels (16-18 Kilojoules) had similar strength. Slightly narrower welds (produced at maximum speeds for the small 10 KVA welder and representing 12 Kilojoules per unit of weld) showed proportionate increases in strength. The work reported herein has been accomplished on .250 inch 2219-T87 using a 10 KVA welder and is being continued using a 15 KVA welder to further reduce time-temperature effects, increase power concentration (i.e., produce a narrow weld) and join thicker material.

INFORMATION CATEGORY

Unclassified

ALG/MB

Authorized Classifier Date

INTRODUCTION

During 1964 Westinghouse engineers had completed a systems engineering study aimed at developing an electron beam welder specifically for the demanding conditions of non-vacuum welding. This approach not only freed the electron beam process from the confinement of a vacuum chamber but also provided the gun with some of the flexibility of an automatic TIG welding head.* Further, limited tests indicated that the unit might show a number of advantages over conventional arc processes (i.e., lower distortion, less heat input, higher welding speeds, etc.).**

On June 15, 1965, a contract was initiated between NASA Marshall Space Flight Center (Welding Engineering Branch) and the Westinghouse Electric Corporation. Phase I of this contract involved a welding engineering study. Phase II, which is not within the scope of this report, required construction of a light weight, portable non-vacuum electron beam welding head, manipulator and enclosure.

SCOPE

In order to meet the objectives of Phase I, two preliminary experimental studies have been undertaken and completed. These were carried out on an available 10 KVA laboratory welder. The findings will be translated to the demonstration of the welding capabilities of the 15 KVA unit and reported separately.

This report covers the findings of the 10 KVA studies which have been divided into the following series of experiments:

Task A - The Westinghouse 10 KVA non-vacuum electron beam welder was applied to the study of the relationship between welding procedure details (Part I, Task A Section 1) and the achievement of the radiographic quality established in ABMA-


* J. Lempert, J. Lowry, F. Seaman, C. Williams, "A Compact Non-Vacuum Electron Beam Welder" Proceedings of Electron and Laser Beam Symposium, 1965, p. 393.

** F. Seaman, J. Lempert, J. Lowry, C. Williams, "Joining 2219 Aluminum Alloy with the Westinghouse Non-Vacuum Electron Beam Welder" 9th National Symposium "Joining of Metals for Aerospace", Society of Aerospace Materials & Process Engineers, Nov., 1965.

PD-R-27A, Class 2 (and other standards as set forth in ABMA-PD-W-45). This work is discussed in Part I, Section A-2,

Task B - The above relationships were applied to the 10 KVA welder and as-welded mechanical properties determined (discussed in Part II Task B).

EQUIPMENT

The 10 KVA laboratory unit on which welding tests covered by this report were conducted is shown in Figure 1. This welder (unlike the XWEB 15121 unit being built in Phase II of this contract) is a stationary device designed to test development components. It is mounted in a lead cabinet having a lead glass window in the access door to permit viewing of the weld. Referring to the photograph, the cylinder at the top of the gun houses an oil-insulated section designed to permit the use of high voltage cables as a means of feeding power to the gun. The section of the unit marked by the Westinghouse trade mark  is the acceleration chamber which houses the cathode assembly. The electron beam is accelerated and electrostatically focused in this region using voltages up to 150 KV. The magnetic lens may be observed directly below. The exit orifice of the gun is housed in a cylindrical lead enclosure and can be observed in the center of the picture immediately above a rack and pinion-driven cart situated directly underneath the gun.

Electrons are released from the cathode of the gun and focused through differentially pumped orifices by a combination of electrostatic and electromagnetic electron optical systems. A positive pressure is applied at a special gas protection orifice which is located just below the exit orifice of the gun producing the flow of gas to the work area which directs particulate matter and vapor away from the nozzle. This orifice protection system minimizes contamination of the vacuum system. The use of the protective gas nozzle also permits control of the atomic number of the gas which is pumped into the vacuum system.

The stainless steel fixture, Figure 1A, (essentially parallel plane surfaces spaced about 1/2 inch from the center line of the weld) is placed on the power-driven cart directly underneath the gun. Using the adjustable table below the cart, the work can be moved vertically through the nominal working range of the process (1/4"-1/2" gun-to-work piece spacing).

MATERIAL

Material for the program was 2219 aluminum alloy furnished in the T87 condition. The nominal chemical analysis was as follows:

Typical	Si	Fe	Cu	Mn	Mg	Zn	Ti	V	Zr	Other	
Percent	.20	.30	5.8/6.8	.20/.40	.02	.10	.02/.01	.05/.15	.10/.25	Total	ppm
(Maximum unless other- wise stated)										.15	.08/.23

*By analysis

The mechanical properties of each of the 48" x 96" sheets from which test panels were cut have been determined. The results reported by NASA-MSFC, Manufacturing Engineering Division Test Request No. 38 are as follows:

TENSILE STRENGTH AVERAGES

Thickness (Inches)	Ultimate (psi)		Yield (psi)		Elongation (%)	
	Longitudinal	Transverse	Longitudinal	Transverse	Longitudinal	Transverse
.250	66,160	66,560	52,500	50,670	15.9	14.4
.354	69,310	69,450	57,120	55,590	14.2	--
.500	69,376	69,620	56,825	56,998	15.4	14.6

Tensile tests were also performed by WANL on panels of each of the several thicknesses of test material and are as follows: (All tests were taken in the transverse direction)

Identification	Thickness (In.)	Ultimate (psi)	Yield (psi)	.2% Offset	Elongation % in 2"
*1	.250	64,840	49,920		13.0
*1a	.250	64,880	50,030		12.0
**2	.250	68,380	54,545		10.5
**2a	.250	68,390	54,010		12.0
*3	.350	71,265	56,560		11.0
*3a	.350	68,790	56,225		12.0
*4	.500	70,300	48,500		10.5
*4a	.500	70,300	50,000		9.5

* Material from 1st shipment received.

** Material from 2nd shipment received.

PART I TASK A

USE OF A 10 KVA WELDER TO STUDY BASIC RELATIONSHIPS BETWEEN PROCEDURE DETAILS AND WELD QUALITY

In Task A the existing, demountable 10 KVA welder (Figure 1) was applied to study the relationships between welding procedures details and the achievement of weld quality. Four hundred welds were prepared and analyzed. This welding was accomplished in five experimental series. The experimental design and the findings of each series are discussed under a separate heading in the following sections:

Section A-1: Covers the relationship of procedure details such as power, speed, focus (lens current), gun-workpiece distance to the physical features of the weld. These features include contour of the upper surface, underbead drop-through and penetration.

Section A-2: Deals with various means for controlling porosity.

Section A-1 Relationship Between Physical Features of a Non-Vacuum Electron Beam Weld and Machine Settings

INTRODUCTION

A four factor experiment was designed to establish the relationship between the physical features of the weld and machine settings using the following controlled variables (or factors):

Power (A): 2 levels were tested (both at 140 KV)

3.6 KW

6.0 KW

Gun-Work Piece Distance D_T (B): 3 levels were investigated

$D_T = 3/8"$

$D_T = 7/16"$

$D_T = 1/2"$

Process Speed (C): 3 levels for physical data

B/M = Bench Mark (i.e., maximum speed to produce full penetration for a given process)

85% B/M = Bench Mark speed minus 15-20% of Bench Mark

70% B/M = Bench Mark speed minus 30-40% of Bench Mark

Lens Current I_L (D): 3 levels - values vary with power level

High: Maximum lens current usable without distorting beam so that it overheats gun.

Low: Minimum lens current usable without distorting beam so that it overheats gun.

Medium: Lens current midway between high and low value for the particular power level.

Four response variables were measured. Three of these variables involved the physical dimensions of the cross section of the weld and were utilized to draw a deductive picture of the behavior of the welding process (particularly the manner in which heat energy was applied to the weldment). Additionally, such dimensions as undercut have a direct bearing on weld quality standards. The three physical variables were:

W_B - Width of the underbead.

T_B - Contour of the top of the weld bead (+ indicates crown; - indicates undercut).

U_B - Contour of the underbead (in terms of extension below the lower surface of the plate).

Porosity was also chosen as a response variable because of its direct relationship to weld quality standards. Furthermore, porosity serves as a telltale relating to thermal conditions in the weld and environmental conditions around the weld. The relationship between machine settings and porosity are discussed in Part I Task A Section A2.

In order to determine the influence of accelerating voltage a supplementary series of tests was run at 110 KV and 3.6 KW (actually 3.7 KW). Only one working distance was evaluated. The results of this series are shown in Tables I-S (for "supplementary"), II-S, III-S, and IV-S.

The values of the individual response variables were subjected to an analysis of variance* in order to determine if any of the observed effects were significant. The results of the analysis are presented as Tables I-IV. Significance, based on 95% confidence, is indicated by the value of the "F-Ratio" in the right hand column. If this value is over the value listed in the following table the effect (i.e., A, B, C, or D), or the interaction between effects (A x B, A x D, etc.), is significant. When significance was indicated for any of the two factor interactions the F ratio was not calculated for the individual main effect.

F Ratio Values Indicative of Significance

1 and 28 Degrees of Freedom - 4.20

2 and 28 Degrees of Freedom - 3.34

4 and 28 Degrees of Freedom - 2.71

While the experiment was designed to detect 3 and 4 factor interactions, none were found to be significant and the variance from these interactions was included in the residual.

In all of the welds produced to establish how machine settings or other mechanical procedure details influence the undercut, drop through and other qualities of the weld the following procedural elements were held constant (except when specifically noted).

1. Test Specimen: All material discussed under Section A-1 is .250 inch thick 2219 aluminum described under "Materials". Four inch strip was sheared from 48" x 96" plates. These strips were in turn sheared to six inch lengths.
2. Type of Weld: Three welds were made in each panel - each at a different lens current (Figure 2 A-G). Welds were produced in the bead-through-plate mode so that variations in joint fit up did not obscure the relationships under study.
3. Tooling: Stainless steel support blocks were used. These were spaced one inch apart to minimize their effect on the observations.

* Davies, O.L., "Design and Analysis of Industrial Experiments," Hafner Publishing Company, New York City, New York.

RESULTS OF SECTION A-1 EXPERIMENTATION

The cross section of all welds resulting from the previously described experiment are shown (with machine settings) in Figures 2 (A - G).

The following paragraphs cover the findings from the portion of the program concerned with the relationship between machine settings (plus gun-workpiece spacings) and the physical shape of the weld (i.e., contour, undercut width, etc.).

Penetration of a non-vacuum electron beam weld thermal energy input into the non-vacuum electron beam weld bead, such as those shown in Figures 2 (A - G) can be divided into two parts (at least). First the concentrated electron beam penetrates the surface of the metal forming what has been described as a high pressure plasma in a cavity within the workpiece. The lower portion of the optimized non-vacuum electron beam weld consists of a narrow fusion zone similar to that associated with the hard-vacuum processes. This zone is a manifestation of the electron beam mode of heat input. Some interaction at the surface of the workpiece heats the surface creating the broad upper portion of the weld. Although the concentrated heat input of the beam emanates from the heart of the workpiece, thermal diffusivity can, at lower speeds, occur to some degree from either the scatter-source or cavity source. Thus process speed determines how much thermal diffusivity dominates the procedure.

Figure 3 illustrates the increasing domination of diffusivity as speed decreased for a given set of parameters. During these experiments this progressive change in fusion zone cross section was recorded for power levels as low as 3.6 KW (where the highest process speed for full penetration was about 25 ipm).

FACTORS AFFECTING BENCH MARK SPEEDS

Since the number of power levels were to be studied, the fastest weld speed at which penetration was observed for any given series of settings was termed the "bench mark" (Figure 3) weld about which the following observations can be made.

1. The bench mark (B/M) represents the lowest heat input obtainable for a one-side one-pass weld.
2. There is a limited range of speed below bench mark (extended downward to about 85% of bench mark speed) where welds in .250 inch material did not exhibit a significant change in fused zone cross section. Whether there is any disadvantage to utilizing this range becomes a matter relating to loss of mechanical properties and is the subject of Task B. As far as weld appearance goes it appears that either the 3.6 KW process or the 6 KW process has a tolerance for speed ranging from 85% of bench mark to the bench mark itself on .250 inch thick material. In order to make the best use of available data all process speeds were stated in terms of a percentage of the bench mark speed for that process. Conventionally tests were run at 85% and 70% of bench mark and at the bench mark.

The following bench mark (D_t 1/2") values were adopted for this program from observations made during the several sets of experiments on .250 inch thick plate:

3.6 KW process	25-27 ipm
6.0 KW process	60-75 ipm
7.8 KW process	95-115 ipm
9.0 KW process	above 115 ipm

In butt welding it was felt to be of practical value to observe if greater power or accelerating voltage could form a full penetration joint at higher speeds or with lower thermal energy. It was also felt that other procedure details might influence the bench marks. Figure 4 graphically displays the various bench marks that were determined for the several measurements. Possibly the increments of working distance and speed were too coarse to detect their effect but an explainable trend does not show in the data. The higher power beam (6 KW) seemed most effected by lens current variations when the workpiece was near the gun. The lower power beam had an erratic effect near the gun but a more distinct trend became evident as the workpiece moved away. A review of the welds produced at 110 KV instead failed to reveal any improvement

resulting from one accelerating voltage over the other. Power alone seemed to be the deciding factor as far as penetration was concerned under the conditions of this test.

FACTORS AFFECTING UNDERBEAD WIDTH

Each of the variables A, B, C, and D is significant with regard to its ability to change the width of the underbead with A and B interacting and C and D appearing as main effects of power. As speed was increased the mean value of the underbead width was reduced about 50% as shown in Figure 5 (a single curve can be used since the A x C, B x C, and C x D interactions are not significant). Lens current can also be considered in the same fashion and its effect can be seen in Figure 6. Changing lens current from low to medium resulted in little reduction in underbead width. The use of a high lens current apparently imparts a distinct "V" shape to the weld and underbead width is reduced by approximately 50%.

The significance of the A x B interaction in Table I suggests that the influence of working distance (D_T) depends upon the power level. The mean values for underbead width shown in Figure 7 indicate that it is the lower (3.6 KW) power setting at which working distance increases in importance as far as its effect on underbead is concerned.

Since the values investigated approximate boundary conditions for a practical process, it would appear that control of speed deserves a high priority in establishing process reliability where full penetration (as evidenced by an adequate, uniform underbead) is used as a criterion of quality.

The lack of a significant interaction between working distance and lens current (B x D) suggests that the factors which control the width of the bottom of the weld are independent of current density or focal point since these phenomenon presumably do change as distance and lens current are changed.

FACTORS AFFECTING UNDERBEAD CONTOUR

Each of the variables A, B, C, and D is significant with regard to its ability to influence the distance that the underbead extends below the plate according to Table II. Power (A), working distance (B), and speed (C) are all involved in two factor interactions which are discussed below. Lens current appears to moderate independently, Figure 8, and suggests that high lens current (i.e., a beam that is focused nearer the gun) produces the least under-bead drop-through.

Increasing the working distance (Figure 9) from $3/8$ " to $1/2$ " decreases the amount of drop-through. The lower power produces the least drop-through at both distances. At the intermediate distance of $7/16$ " the effect is not as easily described. The drop-through for the high power process is less than at either $3/8$ " or $1/2$ " and is greatest for the low power series, exceeding either $3/8$ " or $1/2$ ".

When the effect of working distance is established with respect to its interaction with the three speeds (Figure 10) that were investigated, the trend toward reduced drop-through with increasing working distance is once more evident at the highest (bench mark) and lowest (bench mark-30% bench mark) speeds. At the intermediate speed, working distance does not appear to have a consistent effect.

FACTORS EFFECTING SURFACE CONTOUR

The control of undercut is a function of each of the variables as noted in Table III. Increasing speed limits the tendency of the metal to drop out of the joint - presumably because the volume of metal that is molten for any significant period of time is minimized by the smaller weld puddle associated with faster welding process. The effect is not severe. Even when speed is reduced 15% the undercut is only .0078 inch. This value is below the confidence level of the experiment and is less than 10% of the metal thickness (a value generally used to denote unacceptable undercut). The results are shown in Figure 11.

The effect of the significant two-factor interaction involving lens current and working distance at the two power levels is shown in Figures 12 and 13. Lens current has a significant effect when the process is operating at low power. Moving the point of focus toward or into

the work increases undercut. As noted back in Table II, drop-through of the underbead is effected in the same manner by lens current. No significant lens current effect was observed with the high power process.

An increase from the closest to the furthest working distance reduces undercut. However, as was the case for the underbead contour, the intermediate point of the low power process shows the reverse trend.

INFLUENCE OF REDUCTION IN ACCELERATING VOLTAGE FROM 140 KV TO 110 KV

The results shown in Tables I-S through IV-S show what happens when the accelerating voltage of the 3.6 KW process is reduced from 140 KV to 110 KV.

Underbead Width: Changing the accelerating voltage per se did not influence bottom width but the influence of speed is significant and appears to be more drastic than was the case when the accelerating voltage was 140 KV. The absence of any effect of accelerating voltage on a dimension such as underbead width that logically can be considered to be penetration sensitive might appear to be an anomaly. However, the data on Table I also indicated that underbead was not sensitive to factors affecting current density or focus and accelerating voltage would fall into the same category.

Porosity: There appears to be little difference in the two accelerating voltages at lower speeds. The failure of the auxiliary shield during the 110 KV bench mark series and its replacement by an unimproved shield may explain the severe porosity encountered at the lower KV value. The 140 KV-3.6 KW series was run with a shield that had been modified to provide improved shielding around the orifice so that no comparison can be drawn with assurance.

Underbead Contour: Lowering the accelerating voltage reduced underbead drop-through. There appears to be an analogy between penetration into a block and underbead drop-through.

Upper Surface Contour: The behavior of the upper surface parallels that of the underbead as accelerating voltage is reduced.

As a general comment, it appears that the lack of significance of the lens current and virtual absence of two-factor interactions suggests that the low accelerating voltage reduces the sensitivity (and perhaps flexibility) of the process. Possibly there are optical effects in force at 110 KV that offset any influence that lens current or any of the two-factor interactions that were observed at 140 KV might otherwise exert.

Once again, as noted in 140 KV welds, changes which intensify and sharpen the beam (i.e., focus) cause metal to be displaced vertically but do not narrow or widen the weld.

DISCUSSION OF SECTION A-1 RESULTS

The results of Task A Series A may be viewed in two ways. First, they provide guidance for the adjustment of procedure details during the optimization of a welding procedure for future applications. Second, the trends described in Figures 5 through 13 can be considered, deductively, to present a picture of the various phenomenon that take place during the progressive fusion and solidification of a joint in an assembly that is being welded by the non-vacuum electron beam process.

With regard to the various thermal phenomena that operate during welding, there is a strong suggestion that some thermal focus phenomena exists outside of the welder and inside of the workpiece. This "point" can be made more diffuse and/or moved toward the top and bottom of the weld by manipulating procedure details. Its location determines the cross sectional shape of the molten pool that forms the fusion zone. The shape of the molten pool, and perhaps other factors, in turn controls underbead drop-through and undercut. The width of the process that produces the molten pool alone seems to control underbead width. Short or long focal positions do not effect it. Thus with this tentative picture the welding engineer can exert a control over these characteristics to suit a particular application.

Section A-2

Relationship Between Porosity and Procedure Details

INTRODUCTION

Control of porosity is essential to the application of this process to aerospace hardware. Such control, in conventional welding processes, places constraints on nearly every feature of the welding procedure and the nature of these constraints must be determined before any procedure can be optimized.

The major culprit insofar as gas porosity in aluminum is concerned is generally conceded to be hydrogen. Hydrogen is quite soluble as nascent H^+ in molten aluminum. The hydrogen in the metal will be rejected in the form of porosity as the metal freezes. The welding engineer must consider three aspects of the porosity problem at all times.

1. Source of the hydrogen.
2. Mechanisms that govern the entrance of the hydrogen into the metal and rejection from the metal in the form of gas nuclei.
3. Growth and floatation (and entrapment as detectable porosity) of the gas nuclei.

The most direct method for reducing porosity appeared to lie within the technology associated with shielding. Improved shielding (with efficient cleaning) minimizes the amount of H^+ available to the melt.

Therefore, the major experiment was designed to improve the shielding and in a subsequent series of trials (not statistically designed experiments) some cleaning variations were investigated.

The previous welds produced by various combinations of speed, focus, and working distance were reviewed radiographically to determine the role of procedural details in permitting growth and floatation.

Radiography was accomplished using the following procedure:

KV = 100	Time = 65 seconds
Ma = 3.5	Film = Kodak M
Distance = 48"	Sensitivity = 2-2T

The film was then read using a 7X glass equipped with scale that could be read to .005 inch. Because the trailing shield tends to pull air into its gas flow when it overhangs the ends of the weld, readings were confined to the center 1-1/2 inches of the four-inch long weld.

RESULTS OF SECTION A-2 EXPERIMENTATION

The following paragraphs cover the findings from that portion of the program concerned with the radiographic quality of welds as it applied to porosity.

ROLE OF MACHINE SETTINGS IN SUPPRESSING POROSITY

All test plates from the factorial experiment described in the previous section were subjected to x-ray examination. The diameter of each indication that could be observed at 7X was recorded and placed in one of the following categories.

<u>Range (inches)</u>	<u>Nominal Diameter (inches)</u>	<u>Volume (inches x 10⁻⁹)</u>
.007 - .015	.005	60
.007 - .015	.010	500
.015 - .025	.020	4,000
.025 - .050	.040	32,000

Thus the information on the film was made amenable to an analysis of variance. Such analysis was carried out using pore diameter and pore volume. The results are discussed in the following paragraphs.

Each of the variables A, B, C, and D is significant with regard to its ability to influence the amount of porosity in the weld. Power level, in general, and speed at high power levels

appear (Figure 14) to have the greatest effects. Both would be expected to exert this effect through such phenomena as freezing rate and thermal gradient. The effect of the two factors, lens current and working distance, which might be expected to influence current density is much less.

Only working distance (B) appears to operate independently (Figure 15). It should be noted that increasing working distance also resulted in an increase in the gap between the inert gas shield and the surface being shielded (from 1/16" to 9/16" approximately) which may have contributed to the porosity.

The effect of lens current on porosity is involved in an interaction with power levels. Figure 16 indicates an insensitivity (or slight suppression of porosity) at the 3.6 KW power levels as lens current is changed from high to low. As the lens current is decreased at 6 KW, porosity increases sharply.

Most notable in both Figure 14 and Figure 16 is the tremendous effect of power.

EFFECT OF SHIELD CONFIGURATION ON POROSITY (SERIES B)

The shields used for all tests described previously (experimentally identified as Series A) were constructed as an accessory to the existing 10 KVA welder. Under these circumstances sealing around the nozzle of the welder was not very effective. The shields overheated at their midpoint. This destroyed the seal by causing a lengthwise bow. In addition to the bowing problem severe oxidation of the diffuser material (steel wool and screen) necessitated frequent changes of the shield so that the experimental variance was high in Series A. Since Series B was primarily concerned with porosity as a function of shield configuration, the nozzle was redesigned to accept mounting plates for the various shield test configurations - a "test bed" which could be tightly sealed to the welder. This test bed was cooled to assure its dimensional stability during tests. Shield configurations that provided a simple, easily studied, gas curtain around the beam were built up from modular components. These were fastened to the test bed with solder. Thus a modification in length or width could be accomplished in a few hours. A bottom view of an outer perimeter and filler-gas manifold soldered on the cooled mounting plate is shown in Figure 17.

Experimental Design: Several features of shield configuration were to be evaluated.

There were:

Length of Shield: 2 levels (7-1/2" and 3-1/2")

Width of Shield: 2 levels (2-1/4" and 1-1/2")

Volume of chambers (gallery) into which gas was introduced: 2 levels
(1/8" and 1/4")

Level of gas flow (for one type of gas): 2 levels (Helium = 100 and 200 CFH)

The total number of tests was reduced to 32 through the use of 1/4 factorial design.

Results: The results (stated in terms of pore volume for various pore-size categories) will be found in Table V. The results are related to shield configurations. All welds were run at 6 KW, 1/2" gun-workpiece spacing, 60 ipm (fast), 50 ipm (medium), and 40 ipm (slow).

Effect of Shield Configuration: Only the distance that the manifold pipes were spaced apart (shield width) was shown to be a significant factor in controlling porosity (Figure 18). The extending of the shield ahead and behind the beam caused no significant effect at these speeds when an analysis of variance was applied. The volume of the gallery chamber into which the gas was introduced prior to being directed onto the surface had no effect on porosity.

EFFECT OF THE ADDITION OF A DIFFUSER AND DISCUSSION OF THE ROLE OF OTHER PROCEDURE VARIABLES ON POROSITY

Qualitative observations of the influence of variables ranging from speed to post cleaning procedures on the formation of porosity emphasize need for strict attention to a multitude of details. In this section some of the effects of details such as the addition of a diffuser in the filler block and other procedure variables will be discussed. Actual radiographs will be used to illustrate the findings. As the Task A program approached a point where optimum procedures had to be selected in order to proceed with Task B, no single parameter such as pore volume could be relied upon alone to relate weld quality to existing specifications.

Figure 19 illustrates the severe porosity that can occur in bench mark welds at relatively high power levels (6 KW) when cleaning and shielding are marginal as was the case in Series A of Task A. Simply reducing the power to 3.6 KW under the same shielding conditions accomplished the improvement illustrated in Figure 20. The responsible phenomena would appear to relate to freezing rate or other factors that control the growth of porosity. Note that the more "V" shaped weld formed when a high lens current was used (upper weld) appears somewhat less porous, reinforcing the role of freezing rate and direction as they relate to pore growth and floatation.

The quantitative observation that moving the parallel inert gas manifolds toward the center line resulted in an improvement, is qualitatively illustrated in Figure 21 (though the weld procedure is comparable to the Fig. 19 6 KW illustration). The improvement resulting when the manifolds were moved together suggests a thermal turbulence in the volume of gas surrounding the beam and weld. When the manifolds were far apart the parallel streams of inert gas failed to meet above the path of the weld. Under these circumstances an open corridor existed ahead of and behind the beam impingement area. Down this corridor air could be drawn into the turbulent volume about the intensely hot welding zone. When the manifolds moved together the parallel streams met ahead and behind the weld so that all gas drawn by convection into the weld zone was furnished by these inert gas streams. Placing a diffuser between the manifolds (i.e., in the corridor) simply reduced reliance upon the meeting of the streams and assured a supply of inert gas directly ahead of the process. The improvement resulting from the diffuser particularly at the bench mark speed is illustrated in Figure 22. A review of the cleaning (mechanical) on this plate indicates removal of less than .001 inch total from both sides - this would not now be considered adequate cleaning. Additionally alcohol was used after cleaning. This practice has been discontinued.

At this point in the optimization effort, blanketing of the weld area apparently was rather effective because the substitution of argon (with its high cross section for electrons) for helium severely altered the penetrating qualities of the process. Thus it was felt that the shield was working and the search for sources of porosity was switched to other areas from which hydrogen might emanate. An analysis of two test coupons from Series B indicated less

than .3 ppm H_2 so that the base metal was not believed to be unduly effecting porosity - particularly the bench mark speed porosity.

Chemical cleaning did not decrease the volume of porosity but appeared to change the nature of the porosity by increasing its size (Figure 23). It may be that chemically cleaning once and then producing the high speed weld, may have very effectively dried the plate so that succeeding welds on the same plate were always somewhat less exposed to moisture. Additionally, alcohol was not used on chemically cleaned welds. Both of these changes from the original mechanical cleaning procedure would reduce sources of H_2 and tend to produce a more favorable picture of chemical cleaning than might be the actual case.

Underbead shielding added to either cleaning methods improved the appearance of the underbead and produced the welds shown in Figure 24. These are among the most acceptable welds even though their numerical rating was not significantly different than those observed for welds without underbead shielding. Underbead protection (20 cfm of helium) also reduced or eliminated an "abrasive" surface condition that had been observed on some underbeads. This condition was sometimes associated with undue porosity in slow welds.

Figure 25 quantitatively analyzes the effect of pre-weld surface cleaning and diffuser use on porosity formation. The data shown are representative of welds made at the 6 KW power level at fast (60 ipm), medium (50 ipm) and slow (40 ipm) speeds.

Several general relationships can be observed in the curves:

- (a) Diffuser - non-diffuser relationship at several speeds
- (b) Mechanical clean - diffuser relationship
- (c) Chemical clean - diffuser relationship

Welds made without the use of a diffuser produced a pore size-quantity distribution curve which is similar at all three speeds. That is, the welds were dominated by the 7-15 mil size pores and contained less than 5 pores per inch of the 25-50 mil size. When the diffuser was used, the dominant size was 15-25 mil at fast weld speeds and shifted to the 7-15 mil size at slow weld speeds.

Use of a diffuser reduced the number of pores in the welds. Comparing the peaks of the curves representing pore size and number in non-diffuser and diffuser welds, as weld speed decreased, the ratio (non-diffuser to diffuser) increased from approximately 3:1 at fast speed to approximately 4.3:1 at medium speed to approximately 5:1 at low speed. On closer inspection of the curve it is shown that the ratio decreases because the number of pores in the diffuser welds increased with increasing speed while the number of pores in the non-diffuser welds stayed constant for all speeds. Thus, the diffuser appears to be less and less effective as speed increased. The decrease in quality of diffuser made welds, as speed increases, substantiates the previously mentioned concept of the manner in which the shield works, namely a supply of gas is introduced directly ahead of the process as well as between the manifolds and that the purpose of the gas is to block air introduced by the motion of the workpiece. As speed increases, this blocking action becomes less effective.

As mentioned previously, diffuser shielded welds revealed a pore peak shift from the 15-25 mil size to the 7-15 mil size as speed decreased. This data is based on both mechanically and chemically cleaned welds. A closer examination of data produced by each of these two surface preparation techniques shows a peak shift in the case of chemically cleaned welds from the 15-25 mil size at fast speed to a 7-15 mil size at medium and slow speeds. Mechanically clean welds showed no noticeable peak at fast speed with peaks at the 7-15 mil size at both medium and slow speeds. The level of total porosity in the case of mechanically cleaned welds was much below chemically cleaned welds at fast speeds, slightly below at medium speeds and essentially the same at slow speeds. The advantage at high speed is one reason mechanical cleaning was selected over chemical cleaning for subsequent work. Chemical cleaning seems to be less reliable and produced very large porosity at higher speed.

DISCUSSION OF SECTION A-2 RESULTS

DISCUSSION

While the several remedies tried above produced welds that could be accepted under actual specifications such as ABMA-PD-R-27A it should be noted that the greatest degree of acceptability was achieved in welds made at speeds representing 85% of the bench mark speed (about 50-60 ipm for 6 KW). On the other hand bench mark welds (60-75 ipm) exhibited marked increases in porosity at these low power levels.

INTRODUCTION

The welding studies of Task A produced at least two procedures that could produce porosity free welds at progressively increasing heat inputs. These were to be compared with the tentative heat input versus strength relationship⁽¹⁾ to determine the applicability of this type of single-parameter relationship to the non-vacuum electron beam weld process. Such a comparison would afford guidance as to methods of improving weld properties, or would indicate that welds were achieving as much as could be expected in terms of the broader perspective set forth in Reference 1.

METHOD

Welds were produced in a bead through plate manner using the following procedures:

Welds 451 & 453	6.0 KW	75 ipm	(Bench mark*)	19 Kj/in/in.
455	6.0 KW	64 ipm	(85% Bench mark)	22.5 Kj/in/in
459	6.0 KW	52-1/2 ipm	(70% Bench mark)	27.6 Kj/in/in

Note: Size of welded plate - 4" x 12"

Welds 409	3.6 KW	27-1/2 ipm	(Bench mark)	31.4 Kj/in/in
411	3.6 KW	25 ipm	(85% Bench mark)	34.5 Kj/in/in
413	3.6 KW	20 ipm	(70% Bench mark)	43.2 Kj/in/in

Note: Size of welded plate - 4" x 12"

A supplementary high speed weld series was also produced by welding from each side of the plate. These two-side, one-pass welds were made under the same conditions of beam geometry (i.e., $D_T 1/2"$)

Welds 481	5.0 KW - 6.0 KW	120 ipm	(8% Overlap)	12 Kj/in/in
478	5.5 KW - 5.5 KW	120 ipm	(16% Overlap)	11 Kj/in/in
473	6.0 KW - 6.0 KW	120 ipm	(24% Overlap)	12 Kj/in/in
477	7.0 KW - 4.0 KW	120 ipm	(8% Overlap)	14 Kj/in/in
475	7.0 KW - 7.0 KW	120 ipm	(60% Overlap)	14 Kj/in/in

Note: Size of welded plate - 4" x 8-1/4"

*Refers to the greatest speed with which penetration is achieved under the given set of procedural details - hence the bench mark weld represents the lowest heat input and, usually, the narrowest weld.

A supplementary series of hard vacuum welds was used to produce modified bead shapes and metallurgical structures. This permitted the application of very low heat input levels but the welding speeds were set equal to the 50 ipm and 120 ipm values used in previous series in order to provide some basis for comparison.

Welds	Hard Vac No. 1	2 KW	50 ipm	9.6 Kj/in/in
	Hard Vac No. 2	3 KW	120 ipm	6.0 Kj/in/in

Finally, a GTA weld produced from two sides of the plate was tested to study a different means of introducing thermal energy at a level that was comparable to the 6 KW process. This weld was identified as 124-13, -15, -17, -19 and was made to following parameters:

390 amps; 11.5 Volts; 60 ipm; 48 ipm wire feed (18 Kj/in/in)

Note: Size of plate - estimated greater than 24" x 24" - produced at NASA-MSFC

The mechanical properties of the joints were determined by removing tensile specimens from the above plates after an evaluation of the radiograph. A summary of the pore volume per unit length of weld is included in the tensile data. The specimens were machined in a "Tree" vertical milling machine to an ASTM E-8-61 (Figure 7) configuration. Normally, the underside bead and/or crown were not removed. When the reinforcement was removed, this fact is noted on the tensile data

Actual testing was accomplished on a Wiedeman Mark G, 60,000 pound capacity, screw driven universal test machine. Elongation was measured by means of a deflector which translates the mechanical motion of the cross head to an electrical output which along with load can be recorded to give an autographic load-elongation curve. The tests were run at a cross-head speed of 0.005 inch/inch/minute through the 0.2% offset yield point and then increased to 0.05.

Strain measurements were accomplished by measuring and recording cross-head movement except on specimen number 505-3 which was fitted with strain gages as a supplementary test to study weld metal behavior. The strain gage measuring equipment consisted of Baldwin-Lima-Hamilton A-7 paperback strain gages used in a two-bridge circuit. Gages were mounted on opposite surfaces of the specimen on the width section of the weld at the gage section to

double the sensitivity of the output. Output of the gages was measured with a Baldwin-Lima-Hamilton model 20 strain indicator and fed into an Electro model 500 X-Y recorder.

RESULTS

Table VI lists tensile properties of both the base material and the several test welds together with appropriate data regarding the quality and condition of the weld.

As shown in Figure 26, the 3.6 KW bench mark welds meet the 42-43 ksi requirements of the heat input-strength relationship postulated in Reference 1. Figure 27 adds the 6 KW data which, for the important bench mark weld exhibited essentially the same strength as that achieved for the 3.6 KW process although the heat input was reduced from approximately 30 Kj/in/in to below 20 and speed increased about threefold (27-1/2 ipm to 75 ipm). For a given power setting, the effect of reducing speed appears more drastic at the higher rate (i.e., for the 50 ipm - 6 KW process).

When the method of welding was changed to a two-side, one-pass weld and heat input reduced to as low as 11 Kj/in/in, strength was increased to the 45-46 ksi range (Figure 28). However, as noted in the weld tensile data represented by open circles (Figure 28), the same strength was achieved by the GTA welds. This GTA weld was made in the two-side, one-pass manner but its heat input per unit of weld was 1.7 times greater than that of the non-vacuum electron beam welds of a corresponding two-side, one-pass configuration. In this instance bead contour was observed to play an important role in the level and location of fracture and may have to become part of any parametric expression.

Finally, the hard vacuum welds must be considered. Once again, two sets of conditions (6 Kj/in/in and 9 Kj/in/in) produced similar strengths. However, the high strengths produced (55-56 ksi) were considerably higher than those encountered previously.

DISCUSSION

The optimum combination of procedural details appears to exist in the low-porosity, highly-tolerant 3.6 KW process. With this process welds meeting the predicted strength-energy relationship can be achieved and the low distortion, low residual stress advantages of the process gained without a major investment in cleaning or shielding. However, while the trend toward higher strengths follows lowered energy input, energy input alone does not define the situation and further work must be done to determine how to achieve maximum strength. Apparently some factor(s) had to be operative other than those embodied in the heat input parameter. A post-test metallographic analysis of the cross section size of the weld and of the metallurgical structure of the cast metal as they relate to the weld failures was carried out to determine what these factors might be so as to guide failure efforts.

Figure 24 relates composite weld width to failure. It would appear that width has a strong effect. Where both heat affected zone and fused weld metal are narrow, strength appears to be gained from the support afforded by the unaffected metal. Brazes gain their strength in much the same manner. When welds from the 120 ipm 5.0 KW and the 6.0 KW process two-side, one-pass process were measured, their width appeared too great to receive much support from the above mechanism but the metallographic structure in the cast area (Figure 30) appears to be somewhat refined when it is compared with the lowest strength welds. In contrast, the weakest welds (those at the lowest speed for the 3.6 KW process) exhibit a structure that suggests a very low cooling rate (Figure 30). Thus there is evidence that time-temperature and geometrical considerations changed in these welds. Both may influence strength though their individual contributions could not be isolated in these tests.

Several data have been reviewed and limited supplementary high speed, short-working-distance tests run to provide a guide for further improvements in strength (Figure 31). These suggest that speeds above 220 ipm might produce depth-to-width ratios ranging from 1.2:1 to 1.8:1. Entering Figure 29 with these ratios suggests that strengths slightly above 48 ksi might be encountered. Reducing working distance has already produced depth-to-width ratios that would provide strengths of 48 ksi. However, adequate shields do not exist to cope with either

the high speeds or short working distances according to radiographs of these supplementary welds.

Development of shielding techniques should be carried out under conditions encountered in a moving welding head such as those encountered in the 15 KVA welder. Further the more powerful unit permits exploration of high welding speeds (Figure 32). Thus, further tests involving high speeds and portable shielding should be carried out on the Phase II welder.

CONCLUSIONS

Each step of the Phase I experimental welding programs has thus far served to illustrate and demonstrate the practical applicability of non-vacuum welding in terms of actual quality standards.

1. At the conclusion of the first section of the experimental program, the machine settings that must be controlled in a detailed welding procedure were clearly identified. These are as shown in Table VII.

2. At the conclusion of the Task A, the influence of practical procedure details and shielding methods on porosity in welds was determined. Welds that are compatible with radiographic soundness criteria were produced in at least one thickness of aluminum.

3. Combining the procedure detail necessary for achievement of an acceptable set of physical characteristics with the details required to achieve radiographic soundness in the third step of the program (Task B) produced weld strengths of 43 ksi (2219-T87 as-welded) in one-side, one-pass welds that are comparable to those produced by high efficiency open arc processes such as GTA. Such strengths were obtained with the 3.6 KW process which has a very high tolerance for shielding and cleaning variances.

4. Supplementary welds produced at 120 ipm from both sides of the joint produced 45-46 ksi strengths comparable to similar joints produced by GTA.

5. A review of the breaking characteristics of the several sets of welds pointed to a strong relationship between depth-to-width ratio and strength. A review of width trends as speed is increased suggests that the powerful 15 KVA unit could potentially produce strengths greater than 46 ksi.

FUTURE WORK

Tasks A and B will be repeated (as Tasks D and E) emphasizing the achievement of narrow welds and using the 15 KVA unit after that unit has undergone a comprehensive demonstration on other thicknesses to establish its working range (Task C). The 15 KVA tests will be documented in a final report.

TABLE I

WIDTH AT BOTTOM (W_B)
ANALYSIS OF VARIANCE

<u>Source of Variation</u>	<u>Degrees of Freedom</u>	<u>Sums of Squares</u>	<u>Mean Squares</u>	<u>F - Ratio</u>
Power (A)	1	17244.91	17244.91	
Distance (B)	2	32150.93	16075.47	
Speed (C)	2	111067.59	55533.80	19.4**
Lens Current (D)	2	45584.26	22792.13	7.95**
A x B	2	19006.47	9503.24	3.32*
A x C	2	706.48	353.24	-
A x D	2	15400.92	7700.46	-
B x C	4	12424.07	3106.02	-
B x D	4	19124.07	4781.02	-
C x D	4	4857.41	1214.35	-
Residual (3 and 4 factor interactions)	28	80229.65	2865.35	
TOTAL	53	357796.76		

* Significant at 95% Level

** Significant at 99% Level

Mean Values for Significant Effects

Grand Mean 168.8

S = .054

2S = .108

<u>Power</u>	<u>Distance</u>			<u>Speed</u>		<u>Lens Current</u>	
	<u>3/8</u>	<u>7/16</u>	<u>1/2</u>			<u>Lens</u>	<u>Current</u>
25 ma	194.4	233.3	132.2	15/40	226.4	H	127.8
43 ma	167.8	147.8	137.2	17.5/50	164.4	M	187.2
				20/60	115.5	L	191.4

TABLE II
UNDERBEAD CONTOUR (U_B)
ANALYSIS OF VARIANCE

Source of Variation		Degrees of Freedom	Sums of Squares	Mean Squares	F-Ratio
Power	(A)	1	492.02	492.02	
Distance	(B)	2	2414.78	1207.39	
Speed	(C)	2	3744.78	1872.39	
Lens Current	(D)	2	2671.44	1335.72	11.3 **
A x B		2	2265.14	1132.57	9.57**
A x C		2	588.48	294.24	--
A x D		2	485.15	242.58	--
B x C		4	2465.11	616.28	5.21**
B x D		4	270.11	67.53	--
C x D		4	415.11	103.78	--
Residual (3 and 4 factor interactions)		28	3313.38	118.33	
TOTAL		53	19125.50		

* Significant at 95% Level

** Significant at 99% Level

Mean Values for Significant Effects

Grand Mean 37.2

S = .010

2S = .020

	Distance		
Power	3/8	7/16	1/2
25 ma	38.8	42.2	21.3
43 ma	52.8	30.0	37.8

	Distance		
Speed	3/8	7/16	1/2
15/40	55.8	55.0	29.2
17.5/50	40.8	33.3	41.2
20/60	40.8	20.0	18.3

Lens Current	
H	27.2
M	42.3
L	41.9

TABLE III
UPPER SURFACE CONTOUR
ANALYSIS OF VARIANCE

Source of Variation		Degrees of Freedom	Sums of Squares	Mean Squares	F-Ratio
Power	(A)	1	1420.91	1420.91	
Distance	(B)	2	1009.60	504.80	
Speed	(C)	2	4127.26	2063.63	32.9 **
Lens Current	(D)	2	942.93	471.46	
A x B		2	514.70	257.35	4.11*
A x C		2	11.26	5.63	--
A x D		2	463.59	231.79	3.70*
B x C		4	553.18	138.29	--
B x D		4	309.84	77.46	--
C x D		4	430.85	107.71	--
Residual (3 and 4 factors interactions)		28	1754.42	62.66	
TOTAL		53	11538.54		

* Significant at 95% Level

** Significant at 99% Level

Mean Values for Significant Effects

Grand Mean -9.91

S = .008

2S = .016

	Distance		
Power	3/8	7/16	1/2
25 ma	-15.0	-21.3	-8.8
43 ma	-12.1	- 3.3	1.1

	Lens Current		
Power	H	M	L
25 ma	-5.2	-18.8	-21.0
43 ma	-2.8	- 7.1	- 4.4

Speed	
15/40	-21.5
17.5/50	- 7.8
20/60	- 0.4

TABLE IV
POROSITY
ANALYSIS OF VARIANCE

Source of Variation		Degrees of Freedom	Sums of Squares	Mean Squares	F - Ratio
Power	(A)	1	3884.52	3884.52	3.59*
Distance	(B)	2	222.11	111.06	
Speed	(C)	2	2133.44	1066.72	
Lens Current	(D)	2	364.00	182.00	
A x B		2	200.70	100.35	--
A x C		2	1128.04	564.02	18.27**
A x D		2	574.37	287.19	9.30**
B x C		4	211.45	52.86	--
B x D		4	113.89	28.47	--
C x D		4	121.33	30.31	--
Residual (3 and 4 factor interactions)		28	864.25	30.87	
TOTAL		53	9818.00		

* Significant at 95% Level

** Significant at 99% Level

Mean Values for Significant Effects

Grand Mean 113.3

S = 55
2S = 110

Power	Speed		
	15/40	17.5/50	20/60
25 ma	13.3	15.6	56.7
43 ma	62.2	205.6	326.7

Power	Lens Current		
	H	M	L
25 ma	36.7	32.2	16.7
43 ma	116.7	227.8	250.0

Distance

3/8	90.0
7/16	110.1
1/2	139.4

TABLE I-S (110 KV)

WIDTH AT BOTTOM

ANALYSIS OF VARIANCE

<u>Source of Variation</u>	<u>Degrees of Freedom</u>	<u>Sums of Squares</u>	<u>Mean Squares</u>	<u>F - Ratio⁽¹⁾</u>
Accelerating Voltage (A)	1	48.35	48.35	--
Speed (C)	2	213.70	106.85	3.73*
Lens Current (D)	2	77.70	38.85	--
A x C	2	50.02	25.01	--
A x C	2	61.69	30.84	--
C x D	4	119.54	29.89	--
Residual (A x C x D)	4	130.57	32.64	--
TOTAL	17	701.57		

* 95% Confidence Level

(1) Tests are made from use of residual variance of previous study. Residual variance of 2865 with 28 degrees of freedom.

Mean Values for Significant Effects

Grand Mean 178.1

Grand Mean of Previous Study 168.8

<u>Speed</u>	
15/20	226.7
17.5/25	150.8
20/30	156.7

TABLE II-S (110 KV)
POROSITY
ANALYSIS OF VARIANCE

<u>Source of Variation</u>		<u>Degrees of Freedom</u>	<u>Sums of Squares</u>	<u>Mean Squares</u>	<u>F - Ratio⁽¹⁾</u>
Accelerating Voltage	(A)	1	122.72	122.72	
Speed	(C)	2	241.00	120.50	
Lens Current	(D)	2	33.33	16.66	--
A x C		2	236.78	118.39	3.84*
A x D		2	8.45	4.22	--
C x D		4	156.67	39.17	--
Residual		4	9.55	2.39	--
(A x C x D)		—	—	—	—
TOTAL		17	808.50		

* 95% Confidence Level

(1) Tests are made from use of residual variance of previous study. Residual variance of 3087 with 28 degrees of freedom.

Mean Values for Significant Effects

Grand Mean 55.0

Grand Mean of Previous Study 113.3

<u>Speed</u>	<u>Accelerating Voltage</u>	
	<u>140-25</u>	<u>110-28</u>
15/20	23.3	40.0
17.5/25	33.3	20.0
20/30	30.0	183.3

TABLE III-S (110 KV)
UNDERBEAD CONTOUR
ANALYSIS OF VARIANCE

<u>Source of Variation</u>		<u>Degrees of Freedom</u>	<u>Sums of Squares</u>	<u>Mean Squares</u>	<u>F - Ratio⁽¹⁾</u>
Accelerating					
Voltage	(A)	1	868	868	7.36*
Speed	(C)	2	853	426	3.61*
Lens Current	(D)	2	486	243	--
A x C		2	103	52	--
A x D		2	453	226	--
C x D		4	481	120	--
Residual		4	513	128	--
(A x C x D)		—	—		
TOTAL		17	3757		

* 95% Confidence Level

(1) Tests are made from use of residual variance of previous study. Residual variance of 118 with 28 degrees of freedom.

Mean Values for Significant Effects

Grand Mean 31.9

Grand Mean of Previous Study 37.2

<u>Accelerating Voltage</u>		<u>Speed</u>	
140-25	38.9	15/20	41.7
110-28	25.0	17.5/25	27.5
		20/30	26.7

TABLE IV-S (110 KV)
UPPER SURFACE CONTOUR
ANALYSIS OF VARIANCE

<u>Source of Variation</u>		<u>Degrees of Freedom</u>	<u>Sums of Squares</u>	<u>Mean Squares</u>	<u>F - Ratio⁽¹⁾</u>
Accelerating Voltage	(A)	1	313	313	4.97*
Speed	(C)	2	1059	530	8.41**
Lens Current	(D)	2	402	201	--
A x C		2	208	104	--
A x D		2	401	200	--
C x D		4	429	107	--
Residual (A x C x D)		4	629	157	--
TOTAL		17	3441		

* 95% Confidence Level

** 99% Confidence Level

(1) Tests are made from use of residual variance of previous study. Residual variance of 63 with 28 degrees of freedom.

Mean Values for Significant Effects

Grand Mean -10.8

Grand Mean of Previous Study -9.9

Accelerating Voltage

140-25 -15.0
110-28 - 6.7

Speed

15/20 -21.7
17.5/25 - 5.0
20/30 - 5.8

TABLE VI

Weld Number	KW	KV	Speed	Bead Removed		U.T.S. (psi)	Y.S. (.2%) psi	Elong. 2"	Red. Sect. Pore Vol.
				Yes	No				
409-1*	3.6	140	BM	25 ipm	X	43,310	29,200	4.5	0
411-1*	3.6	140	85% BM	25 ipm	X	43,320	28,960	4.0	0
411-2*	3.6	140	85% BM		X	42,930	29,020	4.5	0
413-1*	3.6	140	70% BM - 20-25 ipm		X	40,270	28,620	4.0	0
413-2*	3.6	140	70% BM		X	42,730	28,270	4.5	0
451-1*	6.0	141	BM	75 ipm	X	43,060	30,700	3.0	16,500
453-1*	6.0	141	BM		X	42,820	34,870	3.0	37,060
455-1*	6.0	141	85% BM	54 ipm	X	43,040	19,930	3.5	0
455-2*	6.0	141	85% BM		X	42,670	24,710	3.5	0
459-1*	6.0	141	70% BM	52 ipm	X	42,490	27,400	4.0	0
459-2*	6.0	141	70% BM		X	41,890	29,260	3.0	0
2-2A***						68,380	54,545	10.5	
2-2B***						68,390	54,010	12.0	
481/482 (481-1)**	5.0/6.0	109/118	120 ipm		X	44,700	36,700	2.35	3,620
481/482 (481-2)**	5.0/6.0	109/118	120 ipm		X	45,090	37,580	2.45	12,120
478/479 (478-1)**	5.5/5.5	114/114	120 ipm		X	45,760	35,320	2.35	1,240
478/479 (478-2)**	5.5/5.5	114/114	120 ipm		X	45,450	36,360	2.40	5,120
478/479 (478-3)**	5.5/5.5	114/114	120 ipm		X	45,020	37,030	2.15	11,180
473/474 (473-1)**	6.0/6.0	116/117	120 ipm		X	43,210	33,660	2.3	15,680
473/474 (473-2)**	6.0/6.0	116/117	120 ipm		X	43,580	34,380	1.6	7,680
477/480 (477-1)**	7.0/4.0	127/100	120 ipm		X	38,920	36,450	1.45	12,740
477/480 (477-2)**	7.0/4.0	127/100	120 ipm		X	39,550	35,590	2.45	16,560
475/476 (475-1)**	7.0/7.0	126/126	120 ipm		X	41,870	34,550	2.8	4,120
475/476 (475-2)**	7.0/7.0	126/126	120 ipm		X	42,480	34,790	2.75	6,060
Note: Above welds all D _T = 1/2"									
*one-side, one-pass; **two-side, one-pass; ***base metal									
1-1A ⁽¹⁾			50 ipm		X	54,620	44,980	2.5	
1-1B ⁽¹⁾			50 ipm		X	54,470	46,405	3.0	
1-1C ⁽¹⁾			50 ipm		X	55,680	46,780	3.0	
1-2A ⁽¹⁾			50 ipm		X	54,230	44,110	3.5	
1A ⁽¹⁾			120 ipm		X	55,200	46,000	3.0	
1B ⁽¹⁾			120 ipm		X	56,100	44,300	3.0	
2B ⁽¹⁾			120 ipm		X	56,700	(unobtainable slipped)	3.0	
1A-1 ⁽²⁾			120 ipm		X	44,340	33,730	2.0	
1B-1 ⁽²⁾			120 ipm		X	43,860	(unobtainable slipped)	2.5	
124-13 ⁽³⁾				X		43,000	27,000	2.5	
124-15 ⁽³⁾				X		43,300	27,500	3.0	
124-17 ⁽³⁾					X	45,800	31,000	3.0	
124-19 ⁽³⁾					X	46,000	28,000	3.0	

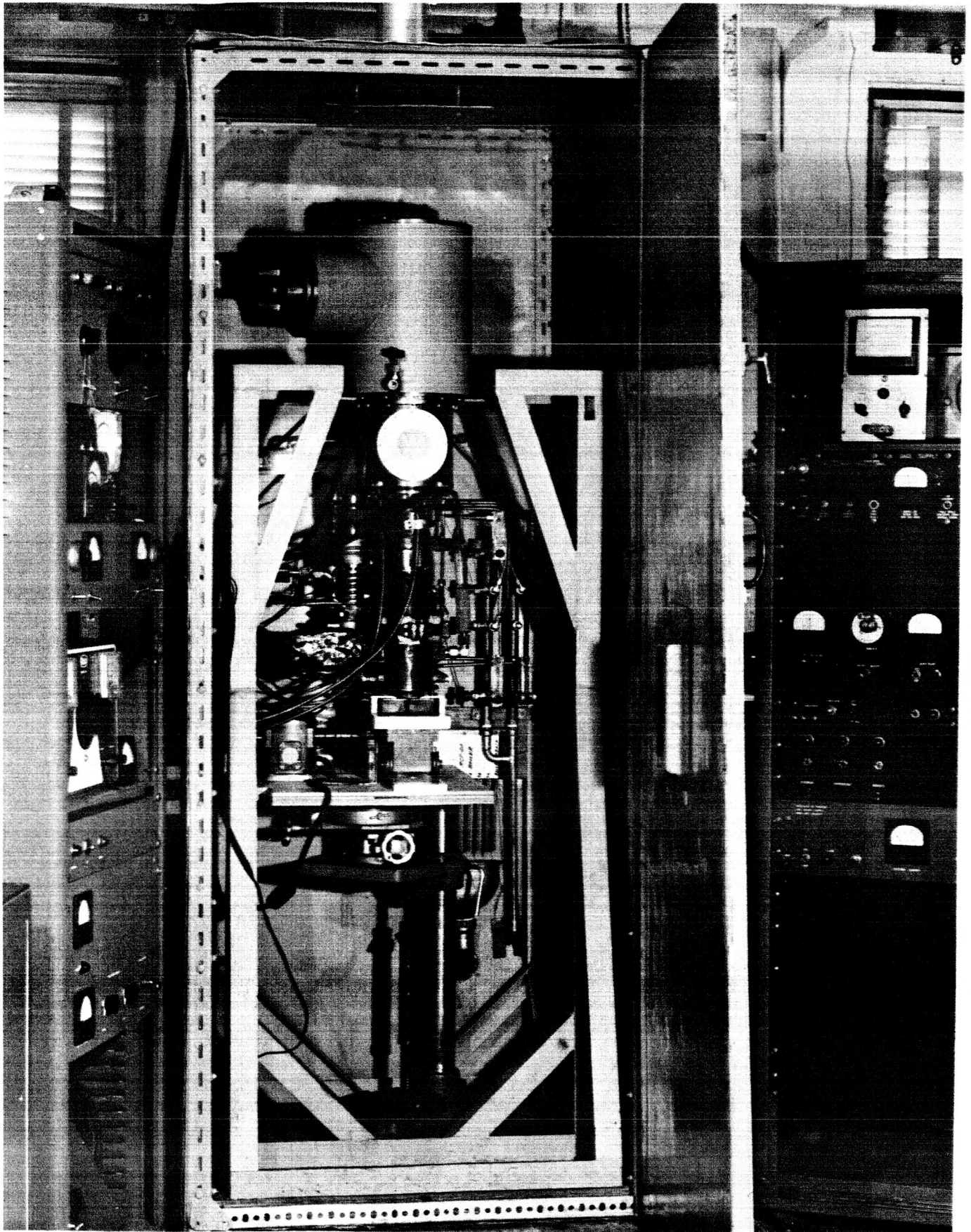
Note: (1) = one-side, one-pass Hard Vacuum Welds
 (2) = two-side, one-pass Hard Vacuum Welds
 (3) = two-side, one-pass G.T. Arc Welds

TABLE VII

<u>Observation</u>	<u>Variable</u>	<u>Interaction-Significant</u>	<u>Effect</u>
Underbead Width	A. Power (3.6 & 6.0 KW)	A. Power and B. Work distance	Changes width. Work distance more important at lower power.
	B. Work Distance (D_T)		Insignificant
	C. Process Speed		Increased speed = decreased width.
	D. Lens Current		Only at high current does width decrease.
	E. Reduction in accel. voltage 140-110		Insignificant
Underbead Contour	A. Power (3.6 & 6.0 KW)	A. Power and B. Work distance	Lower power = least drop through. Greatest drop through at low power and $7/16 D_T$.
	B. Work Distance (D_T)		Increase from $3/8"$ to $1/2"$ = less drop through.
	C. Process Speed	C. Speed and B. Work Distance	Trend to reduce drop through at increased work distance and at highest and lowest speeds.
	D. Lens Current		High lens current = least drop through.
	E. Reduction in accel. voltage 140-110		Reduced drop through.
Surface Contour (Undercut)	A. Power (3.6 & 6.0 KW)		Higher power = less undercut.
	B. Work Distance (D_T)		Increase from closest to farthest = less undercut.
	C. Process Speed		Increased speed = reduced undercut.
	D. Lens Current	D. Lens current and A. Power	Decreasing lens current at low power = increased undercut. No effect at high power.
	E. Reduction in accel. voltage 140-110		Parallels underbead contour behavior.

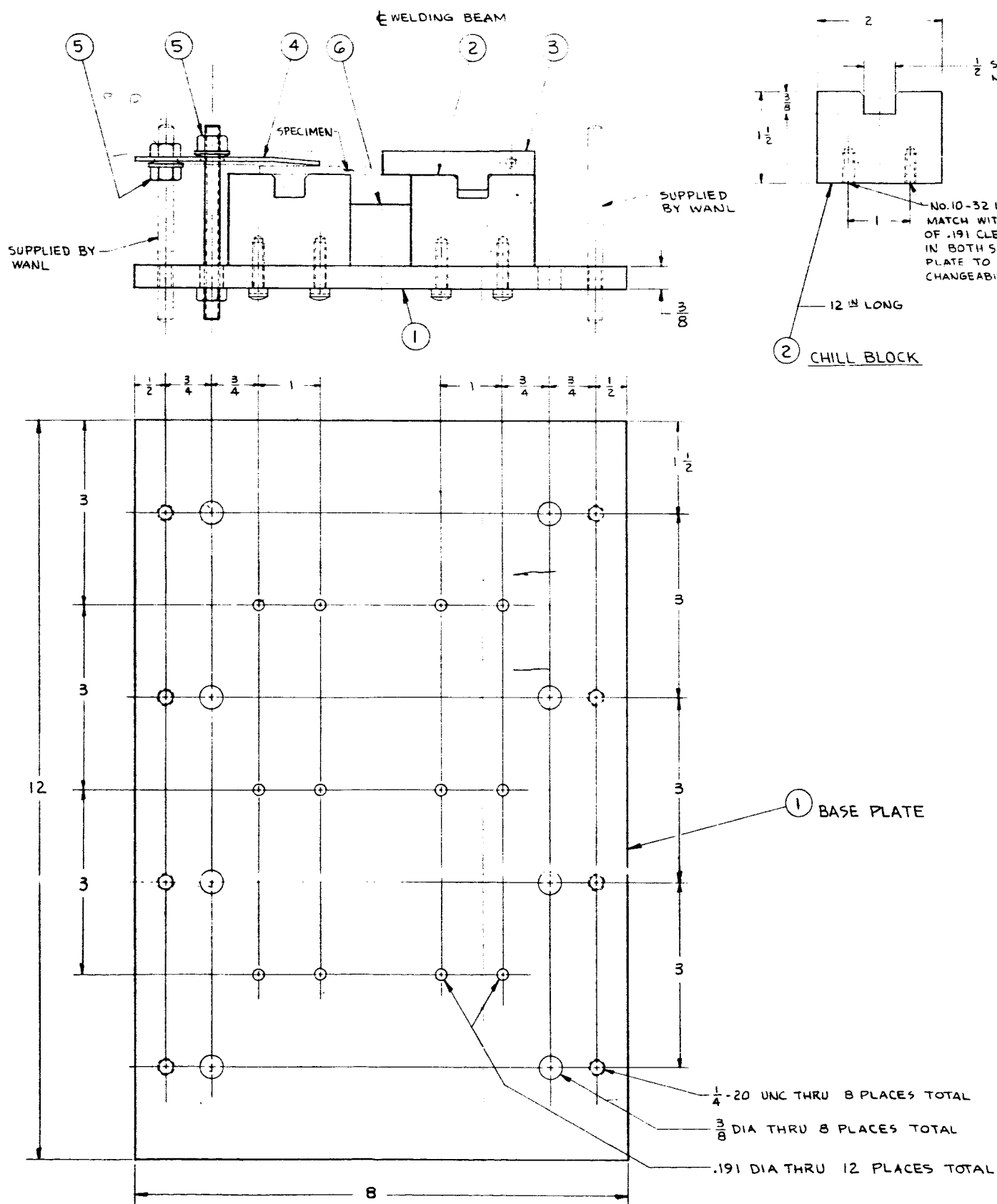
TABLE VII (Continued)

<u>Observation</u>	<u>Variable</u>	<u>Interaction-Significant</u>	<u>Effect</u>
Porosity	A. Power	A. Power and C. Process Speed	Higher power and speed = greater porosity. Higher power level = greater porosity.
	B. Work Distance		Closer distance = less porosity.
	C. Process Speed		Lower speed = lower porosity.
	D. Lens Current	D. Lens current and A. Power	At lower power and high to low lens current = slightly less porosity. At high power and same decrease in lens current = sharp porosity increase.
	E. Reduction in accel. voltage 140-110		Little difference in either 140 or 110 KV.
	F. Shield Configuration		Increasing distance between manifold pipes increases porosity.
	(a) add diffuser		Number and size of pores decreases particularly as speed decreases.
	G. Cleaning		
	(a) Chemical		Only slight increase in pore size.
	(b) Mechanical	Chemical or mechanical clean and underbead shielding.	Slight improvement. Greatly decreases porosity.



WESTINGHOUSE 10 KVA LABORATORY WELDER
USED FOR TASKS A AND B

FIG. 1



E KEYWAY
 NOTE
 IF $\frac{1}{2}$ DEEP
 PATTERN
 RANCE HOLES
 YES OF BASE
 PROVIDE INTER-
 ITY OF CHILL BLOCKS

— THIS FACE TO PARALLEL
 WITH KEY FACES WITHIN .002

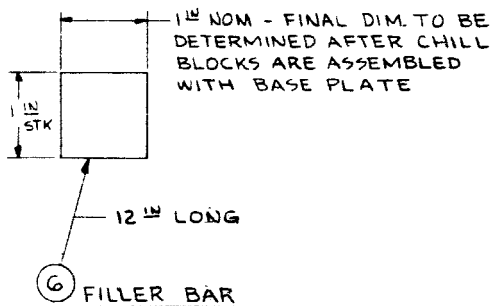
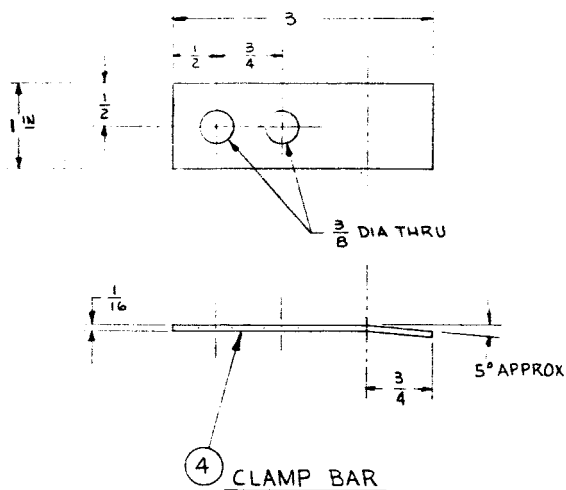
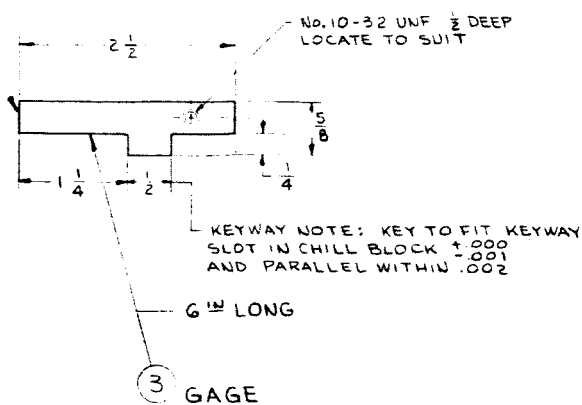


Fig. 1-A

3	6	FILLER BAR		CRES	304	
16	5	CLAMP PIVOT - $\frac{1}{4}$ -20UNC SPHERICAL FLANGED NUT		C.STL	COML	
12	4	CLAMP BAR		CRES	304	
1	3	GAGE		CRES	304	
2	2	CHILL BLOCK		CRES	304	
1	1	BASE PLATE		CRES	304	
QTY.	SYM	ITEM NO.	NOMENCLATURE OR DESCRIPTION	PART OR IDENTIFYING NO.	MATERIAL	SPECIFICATION
REQD						ZONE

LIST OF MATERIALS

UNLESS OTHERWISE SPECIFIED DIMENSIONS IN INCHES DO NOT SCALE				CONTRACT NO.		Westinghouse Astronuclear Laboratory Pittsburgh, Pennsylvania	
TOLERANCES				DATE OF Dwg.	DATE OF Dwg.		
2PL DEC 3PL DEC ANGLES				MAILED	8-17-65		
± ± ±				CHECKED	RELIA. & G. A.		
FRACTIONS $\pm \frac{1}{64}$				DESIGNED	8-17-65		
				ANALYSED	8-17-65		
SPECIFICATION				TYPE	CODE IDENT NO.	Dwg. NO.	
D-SPEC				PCN	14683		
ME-LHA-019				INFORMATION CATEGORY	SCALE 1/1	WT ACT	WT CALC
AUTHORIZED CLASSIFIER				DATE	SHEET 1 OF 1		



Figure 2B

IPM

3.6 KW (110 Kv) 3/8 D₊

1.625x

20

70

71

72

25

53

54

55

25

65

66

69

30

62

63

64

35

59

60

61

40

56

57

58

I(lens)

High

Low

Med

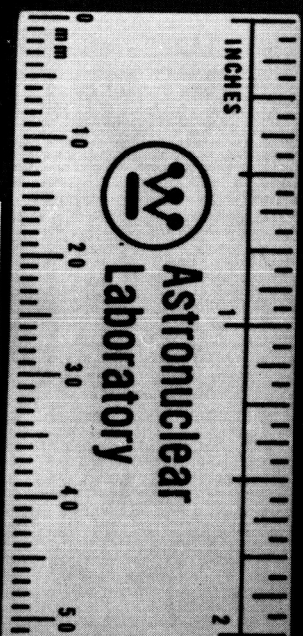


Figure 2A



Figure 2C

IPM

3.6KW (140KV) 1/2D₊

1.625x

15

155

156

157

17 1/2

152

153

154

20

128

129

130

30

125

126

127

40

122

123

124

l(lens)

High

Low

Med

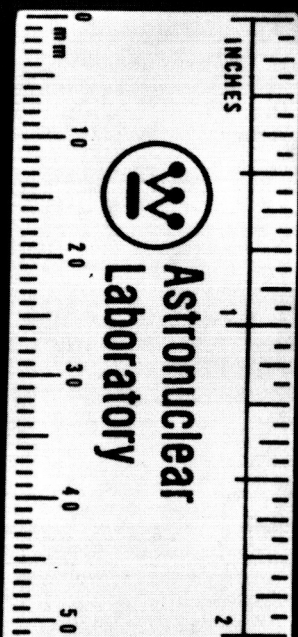


Figure 2D

IPM

6KW

3/8 D_t

1.625x

94

95

96

82

83

84

85

86

87

88

89

90

91

92

93

I(lens)

High

Low

Med

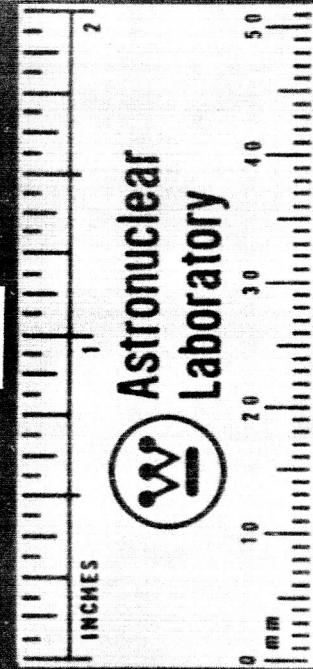


Figure 2E

IPM

6 KW

7/16D₊

2.125x

40

107

108

109

50

104

105

106

60

98

99

100

70

101

102

103

I(lens)

High

Low

Med

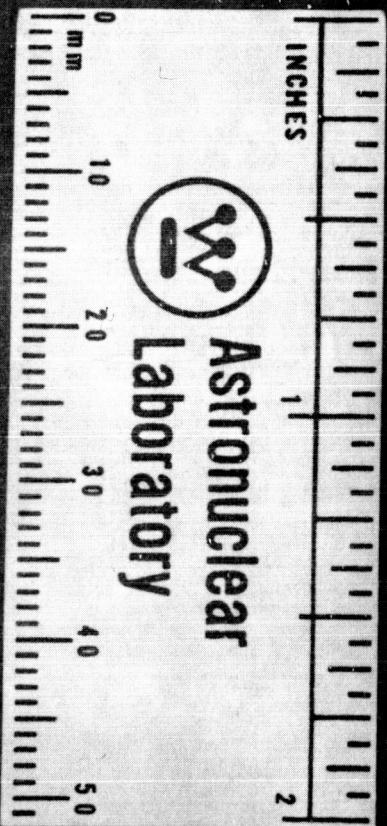


Figure 2F

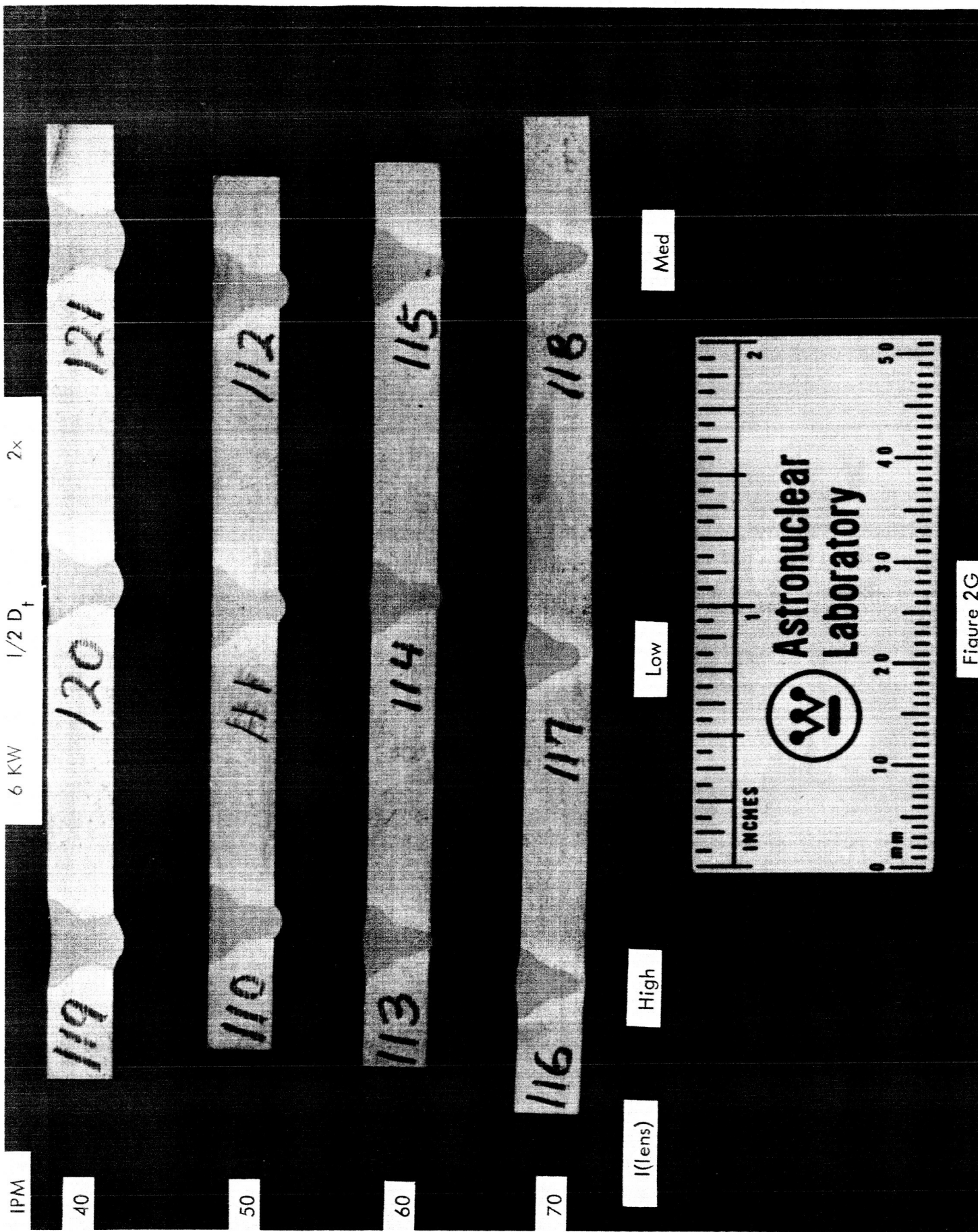
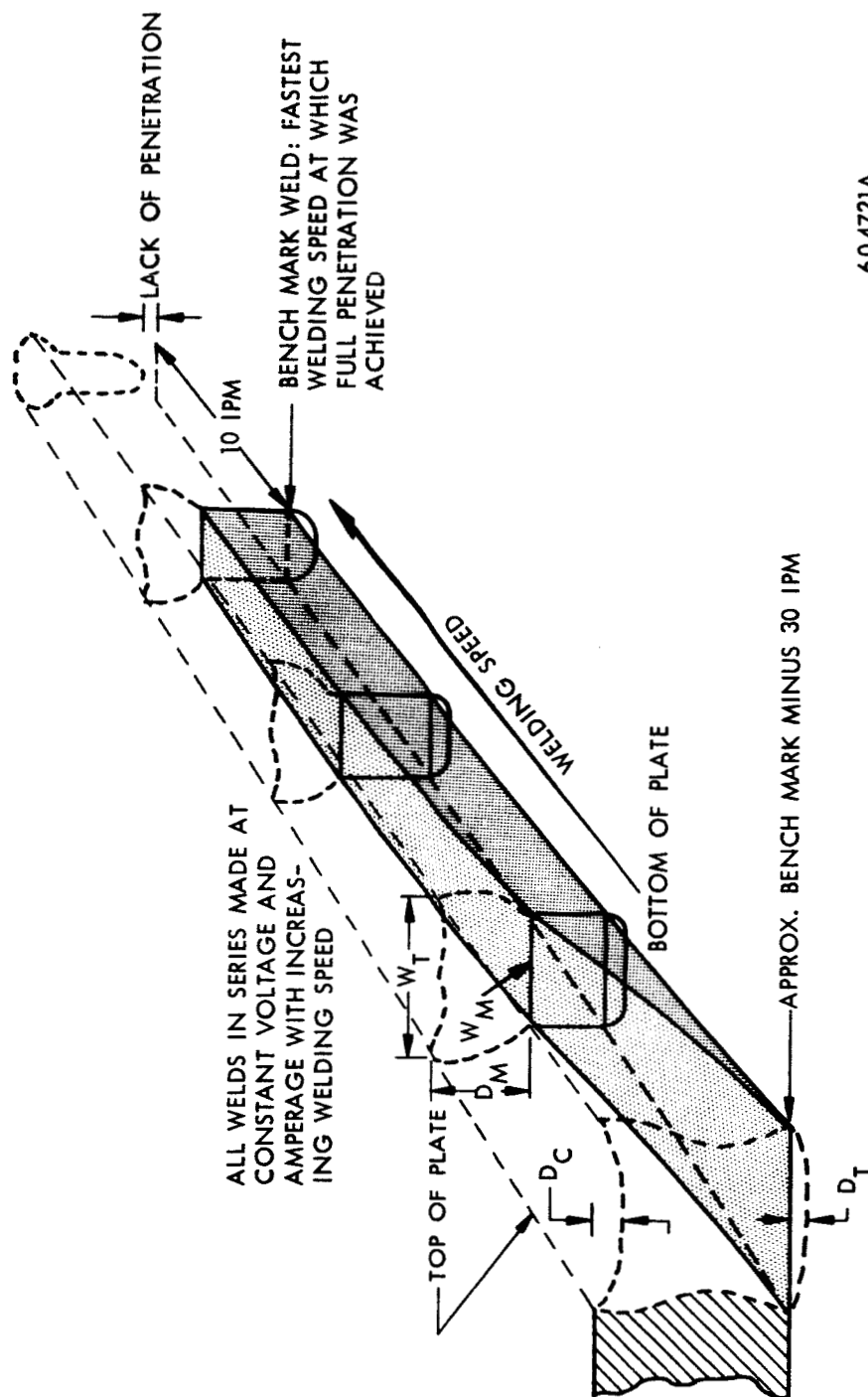


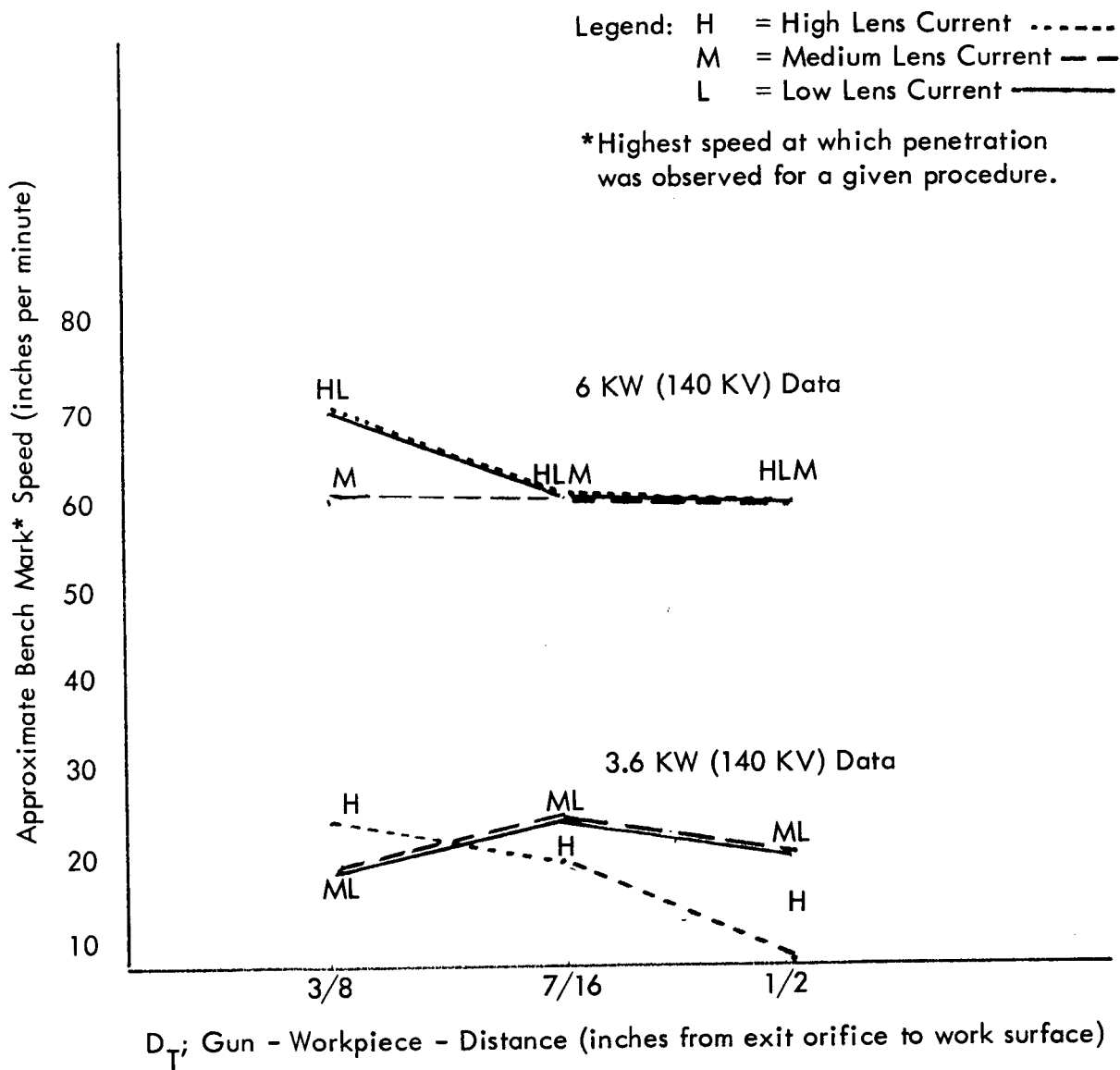
Figure 2G



604721A

DEVELOPMENT OF WELD CROSS SECTION WITH INCREASING SPEED

FIG. 3



EFFECT OF WORKING DISTANCE, POWER, AND LENS CURRENT ON BENCH MARK SPEED

FIG. 4

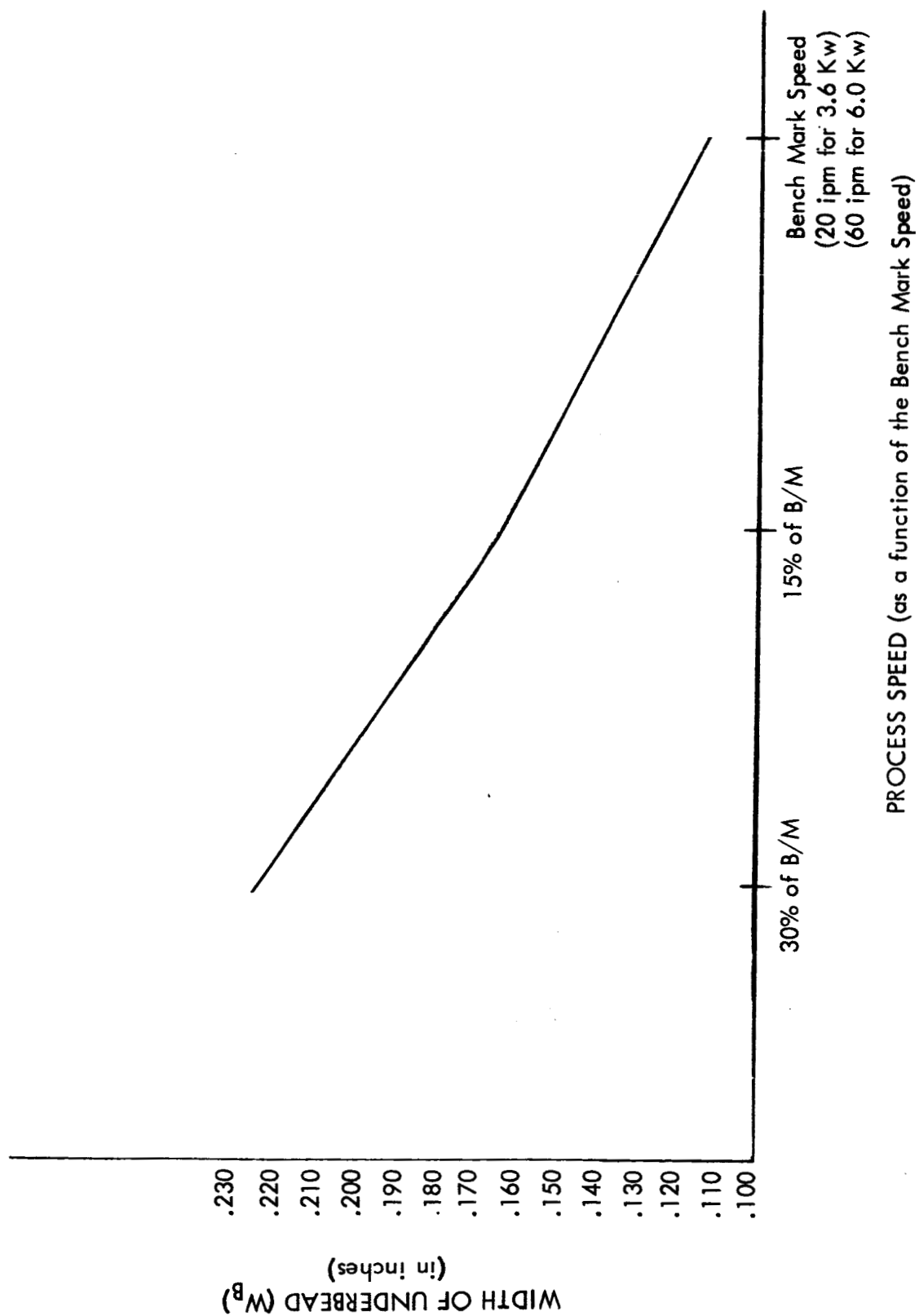


FIGURE 5

UNDERBEAD WIDTH - COMPOSITE EFFECT OF SPEED AT TWO POWER LEVELS
THREE WORKING DISTANCES AND THREE LENS CURRENT SETTINGS

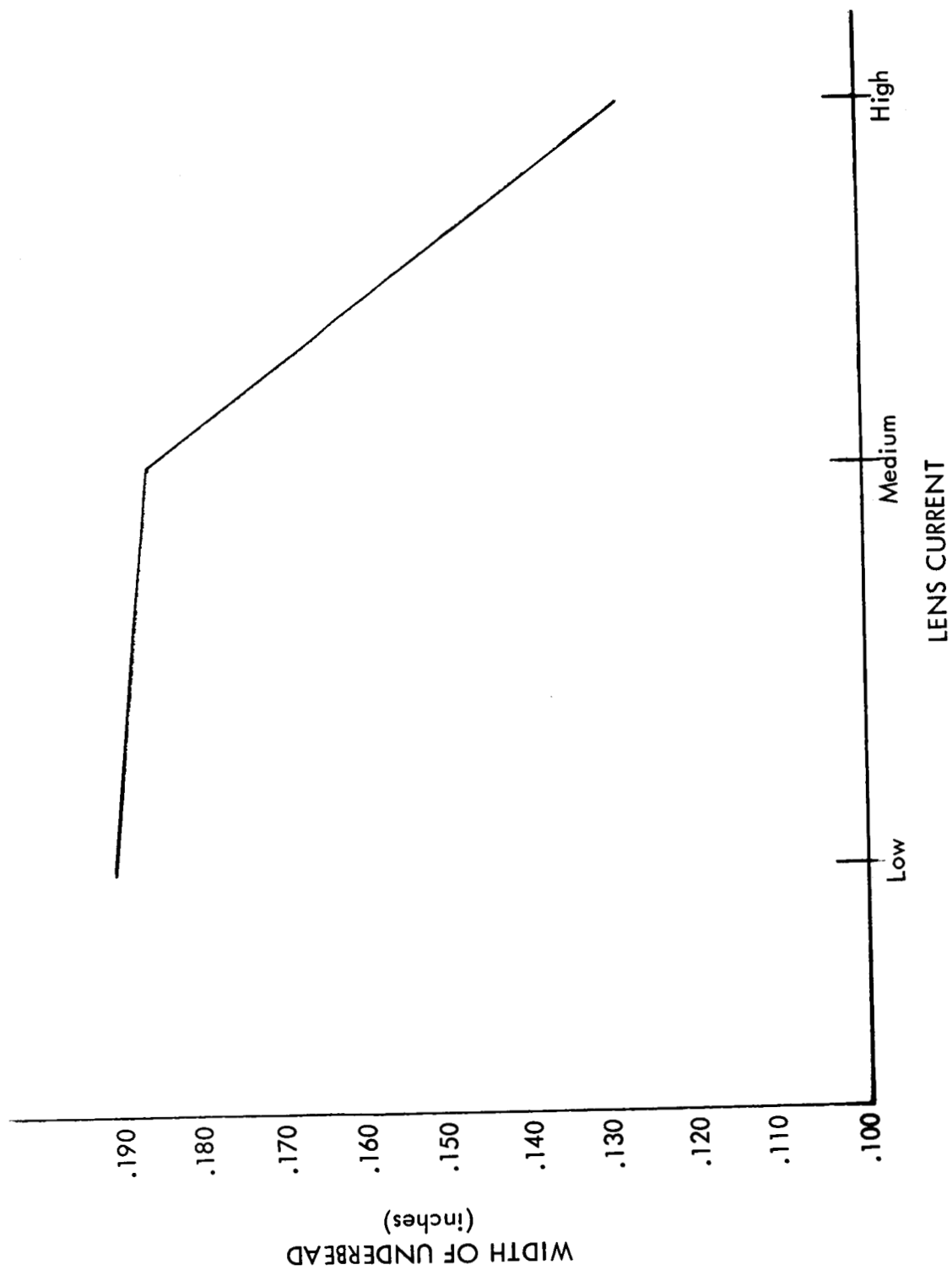


FIGURE 6

UNDERBEAD WIDTH - COMPOSITE EFFECT OF LENS CURRENT AT THREE SPEEDS
THREE WORKING DISTANCES AND TWO POWER LEVELS

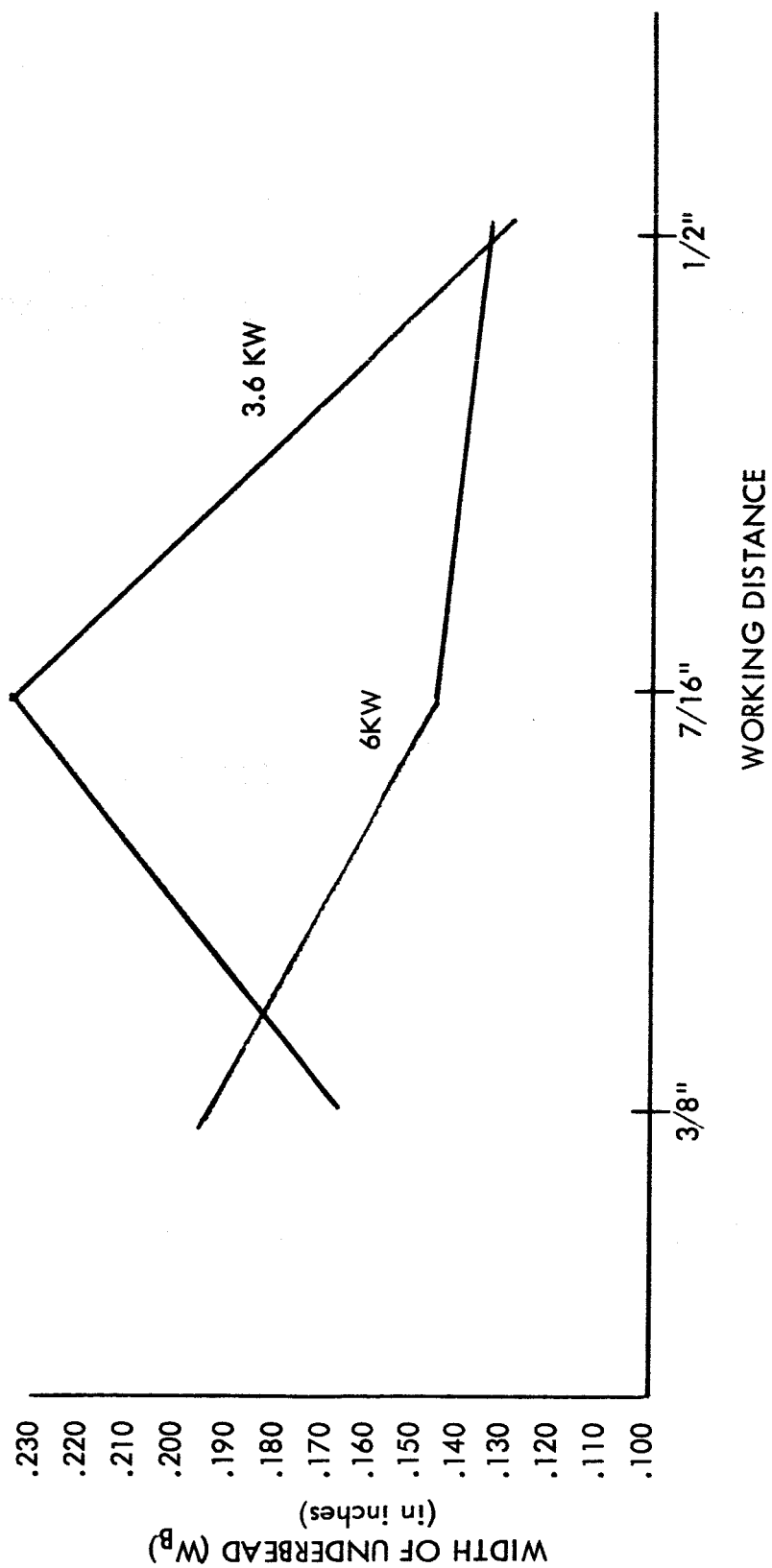


FIGURE 7

WORKING DISTANCE - EFFECT AT TWO LEVELS OF POWER

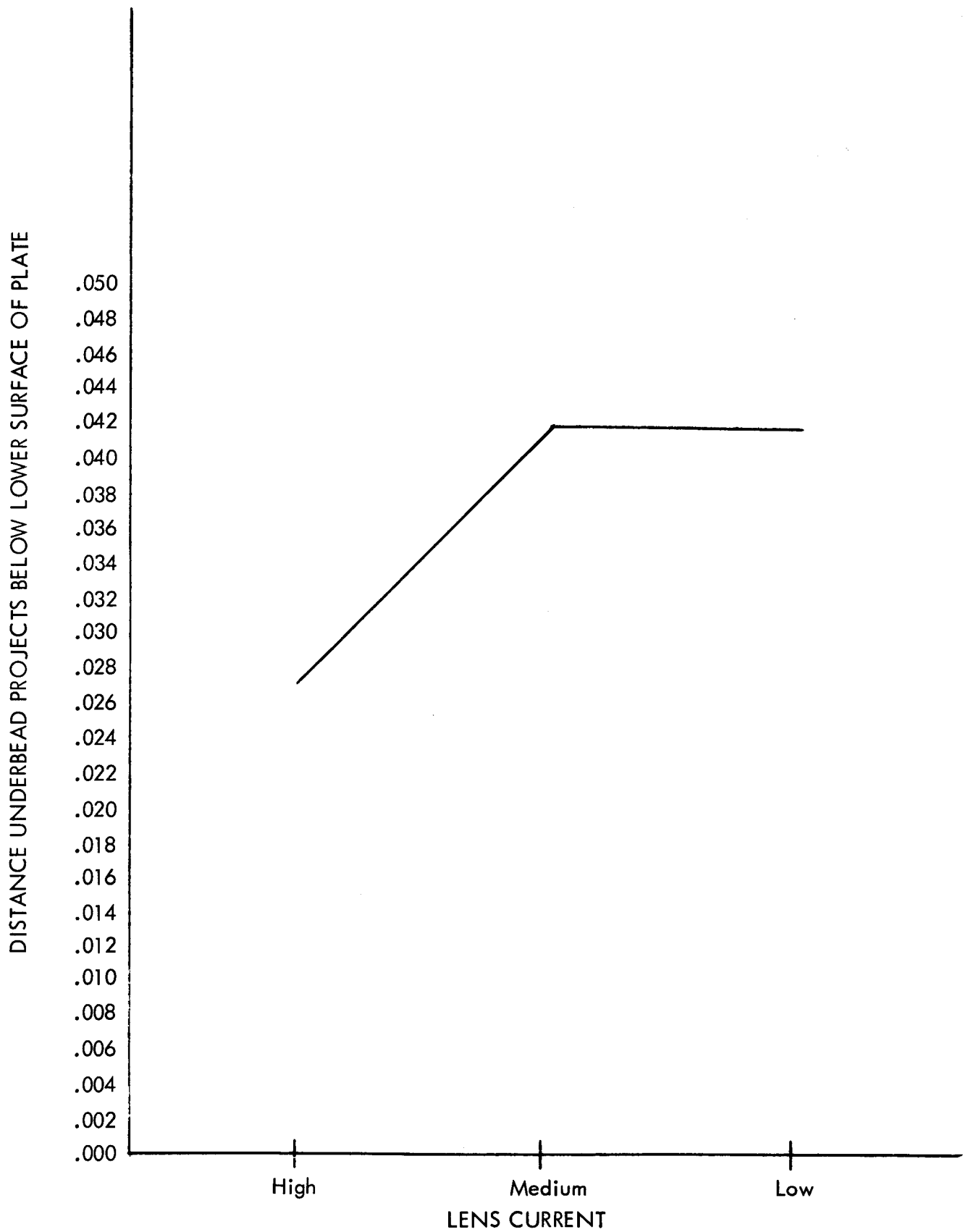


FIGURE 8

COMPOSITE EFFECT OF LENS CURRENT ON UNDERBEAD CONTOUR

DISTANCE UNDERBEAD PROJECTS BELOW LOWER SURFACE OF PLATE

.054
.052
.050
.048
.046
.044
.042
.040
.038
.036
.034
.032
.030
.028
.026
.024
.022
.020
.018
.016
.014
.012
.010
.008
.006
.004
.002
.000

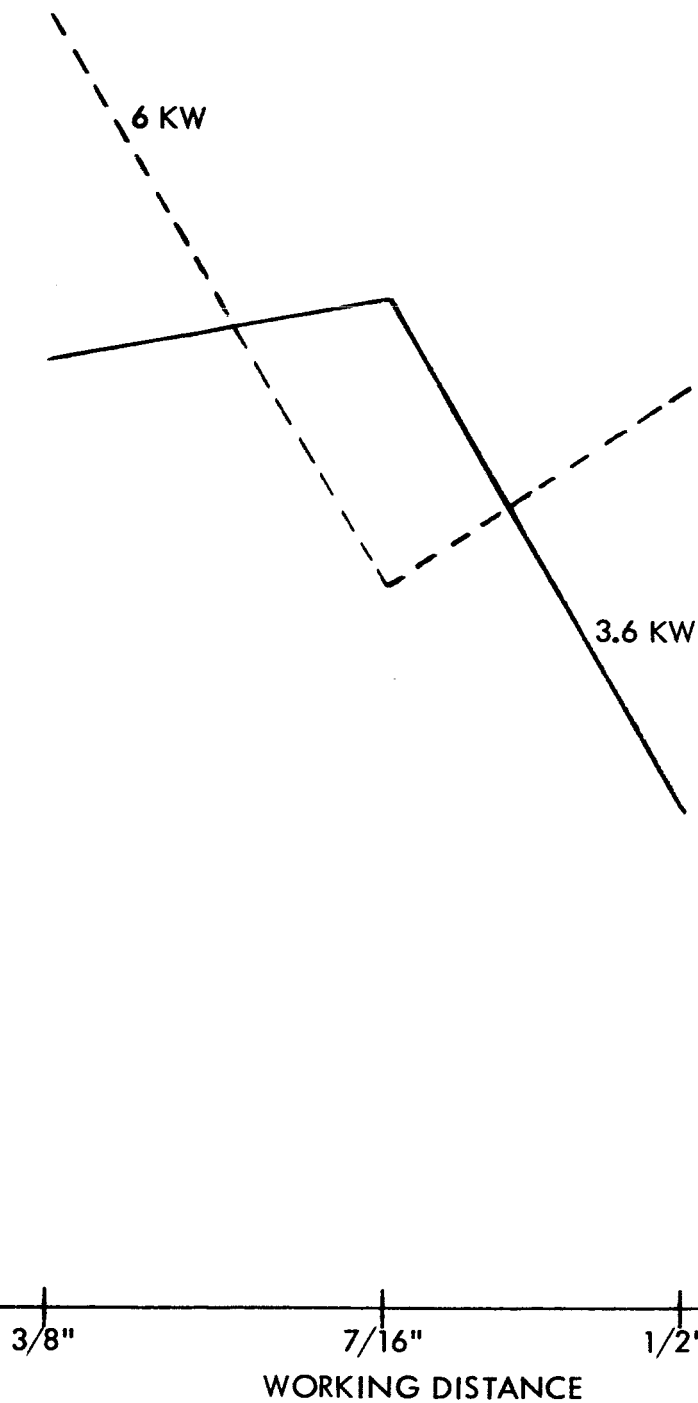


FIGURE 9
THE EFFECT OF WORKING DISTANCE ON UNDERBEAD CONTOUR
AT TWO POWER LEVELS

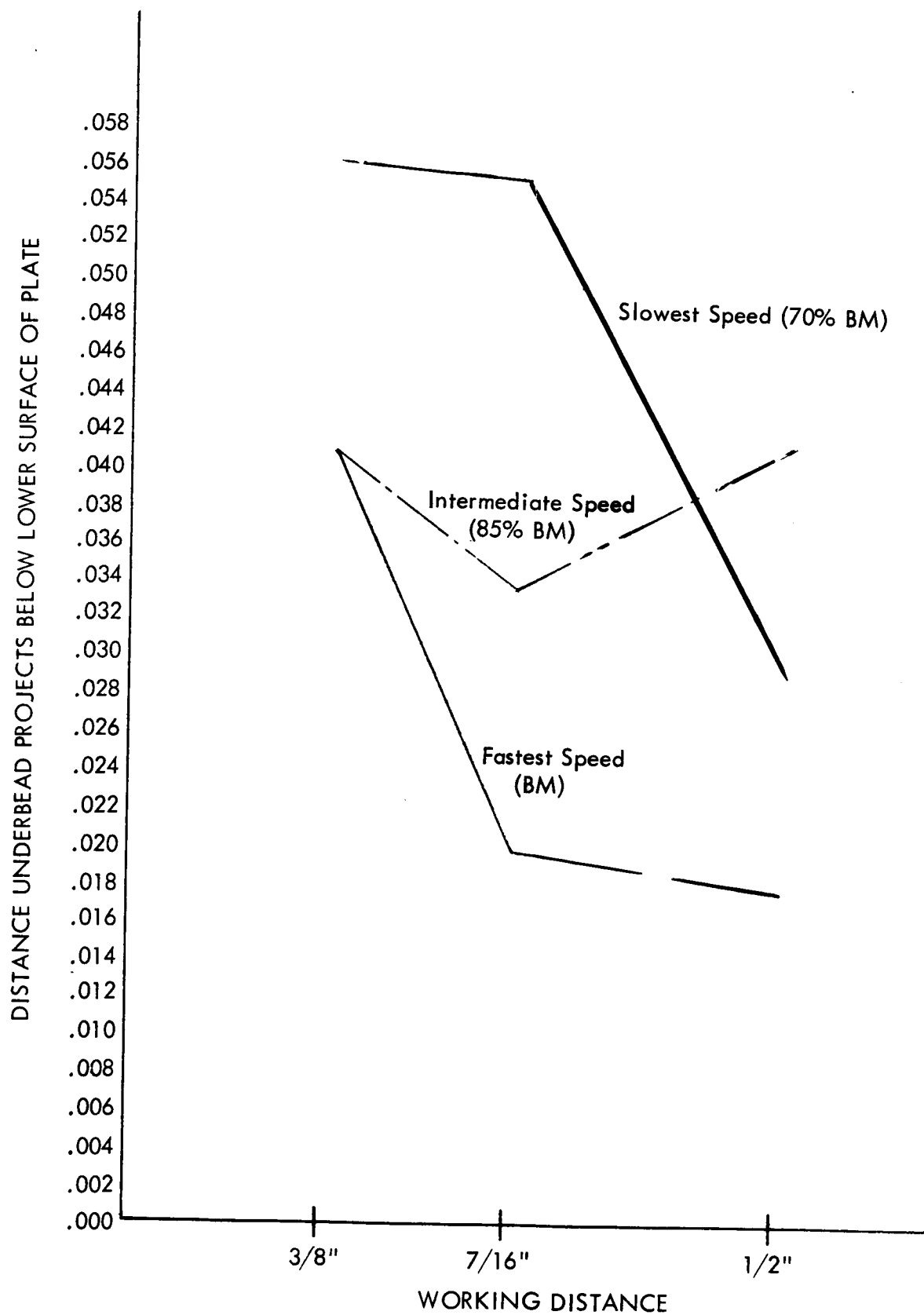


FIGURE 10

EFFECT OF WORKING DISTANCE AT BENCH MARK SPEED
AND AT TWO LOWER SPEEDS

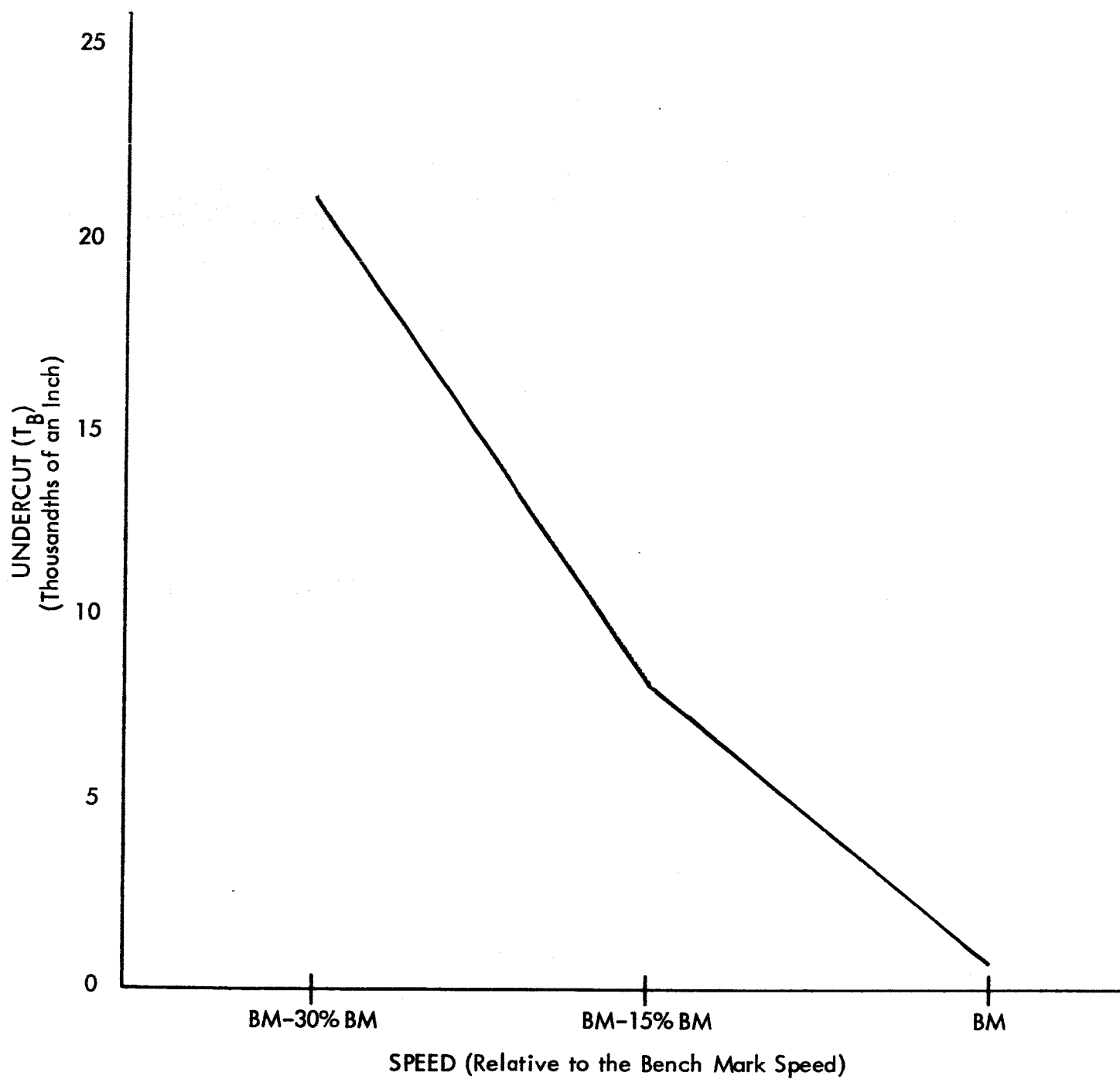


FIGURE 11
SPEED ~ COMPOSITE EFFECT AT TWO POWER LEVELS, THREE LENS CURRENTS
AND THREE WORKING DISTANCES

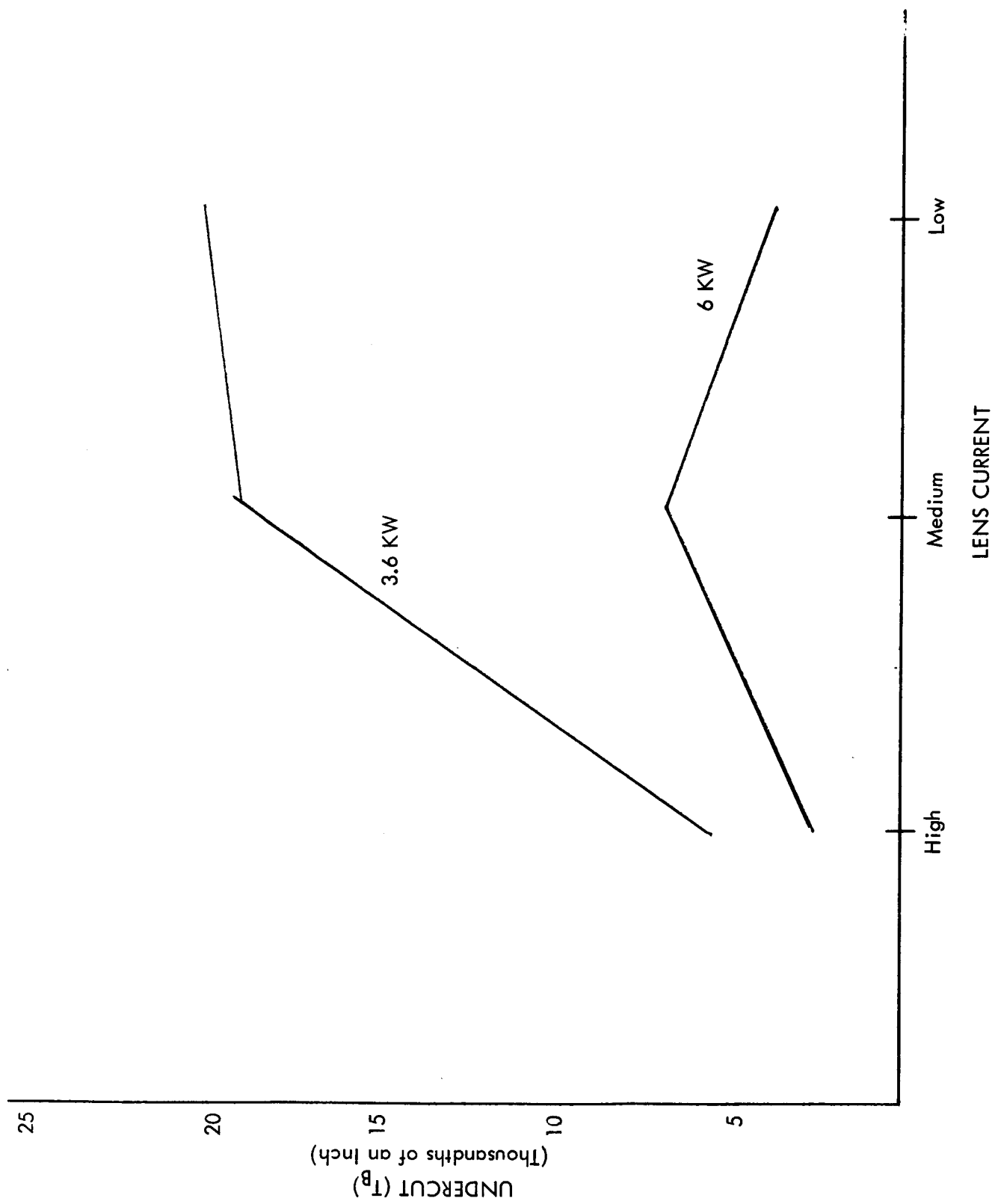


FIGURE 12
EFFECT OF LENS CURRENT AT TWO POWER LEVELS

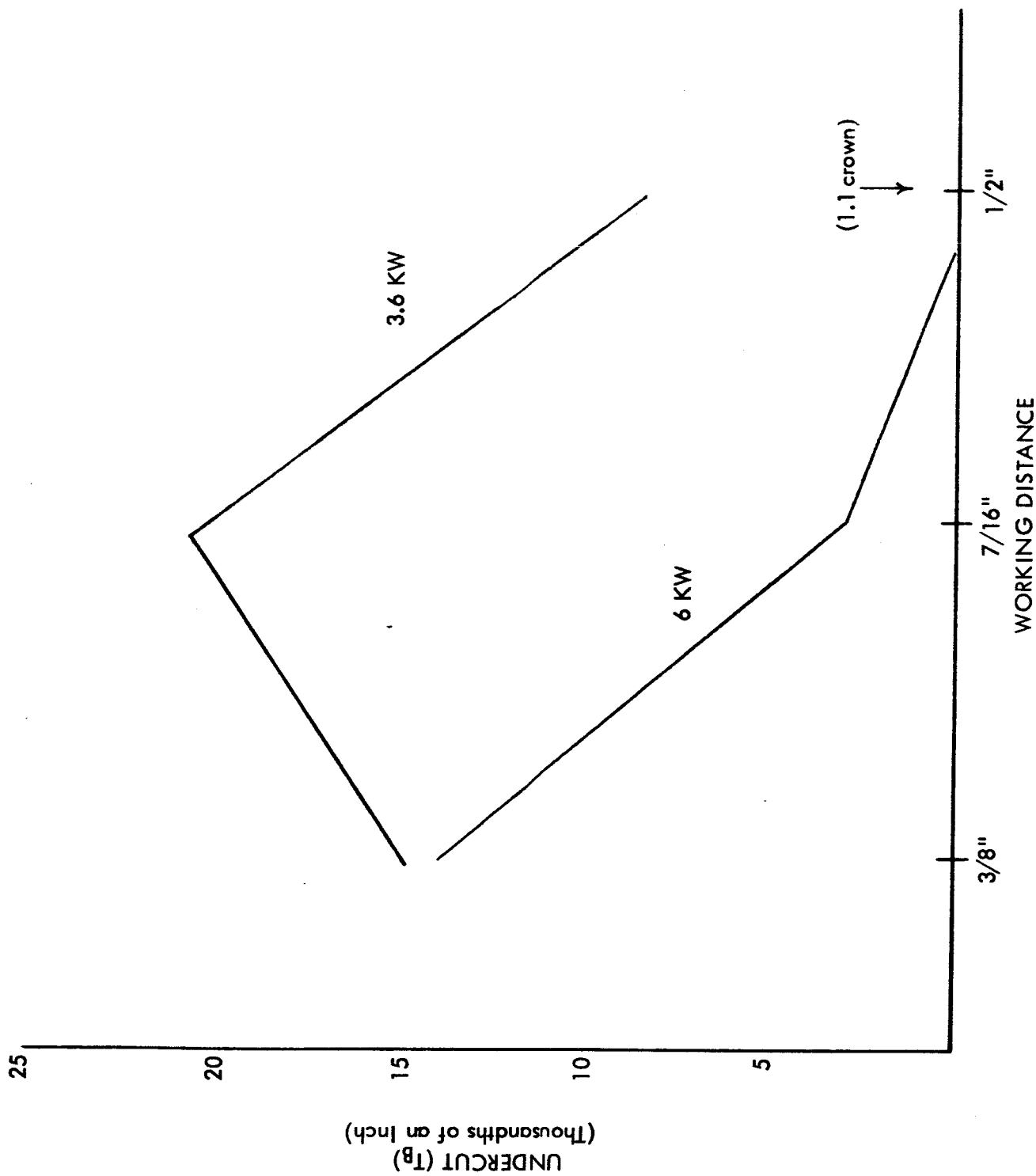


FIGURE 13
EFFECT OF WORKING DISTANCE AT TWO POWER LEVELS

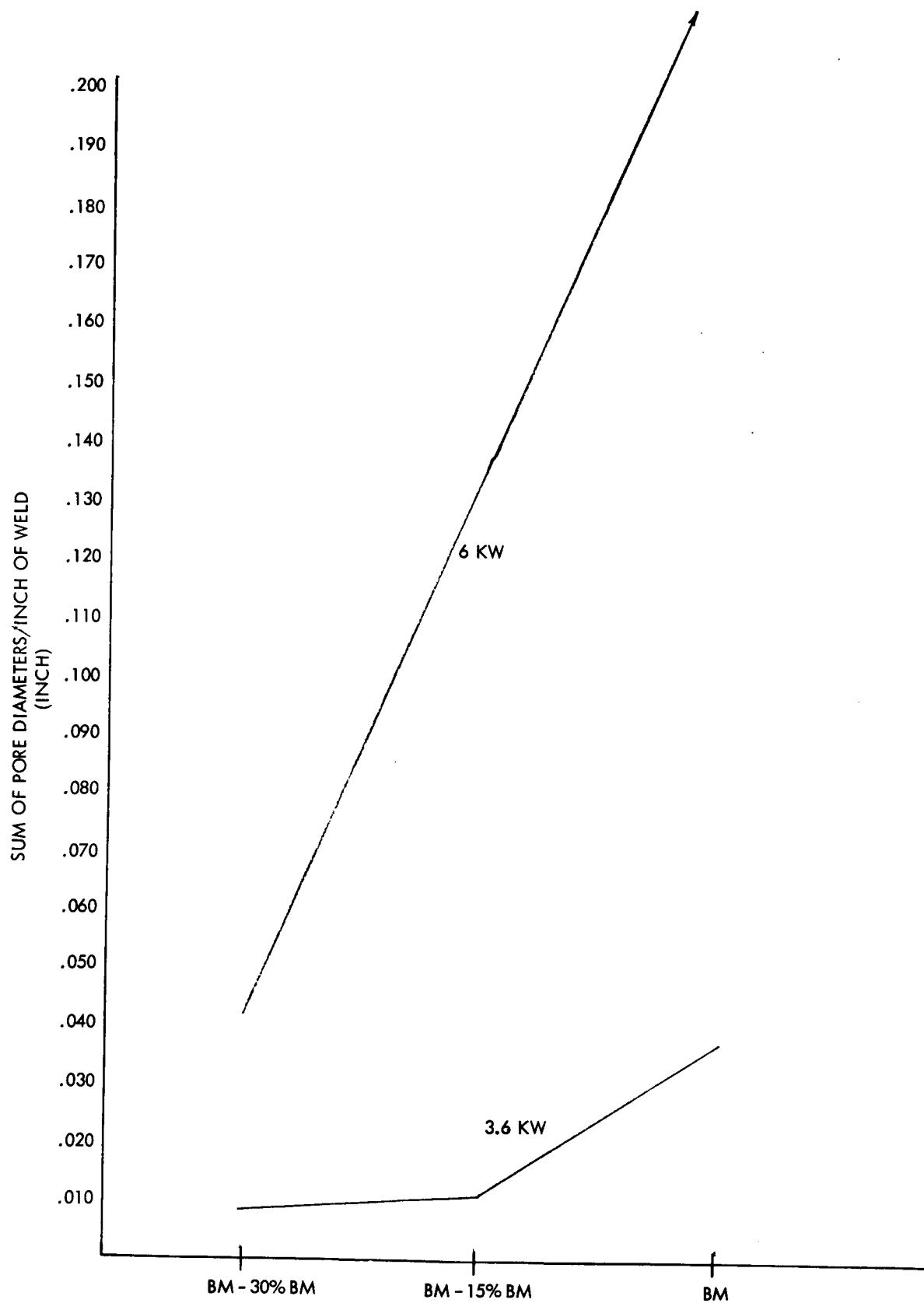


FIGURE 14
EFFECT OF SPEED ON POROSITY AT TWO POWER LEVELS

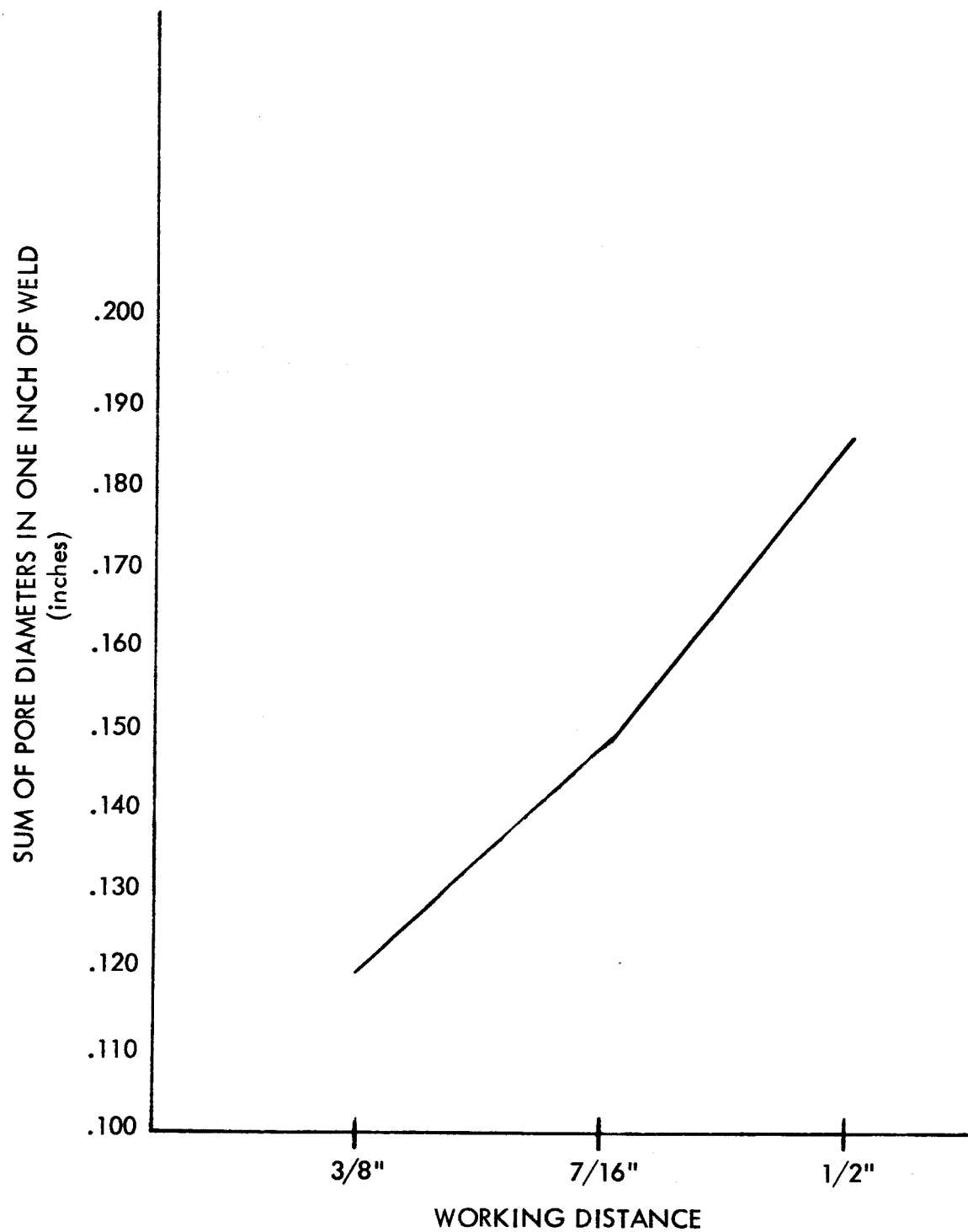


FIGURE 15
COMPOSITE EFFECT OF WORKING DISTANCE ON POROSITY

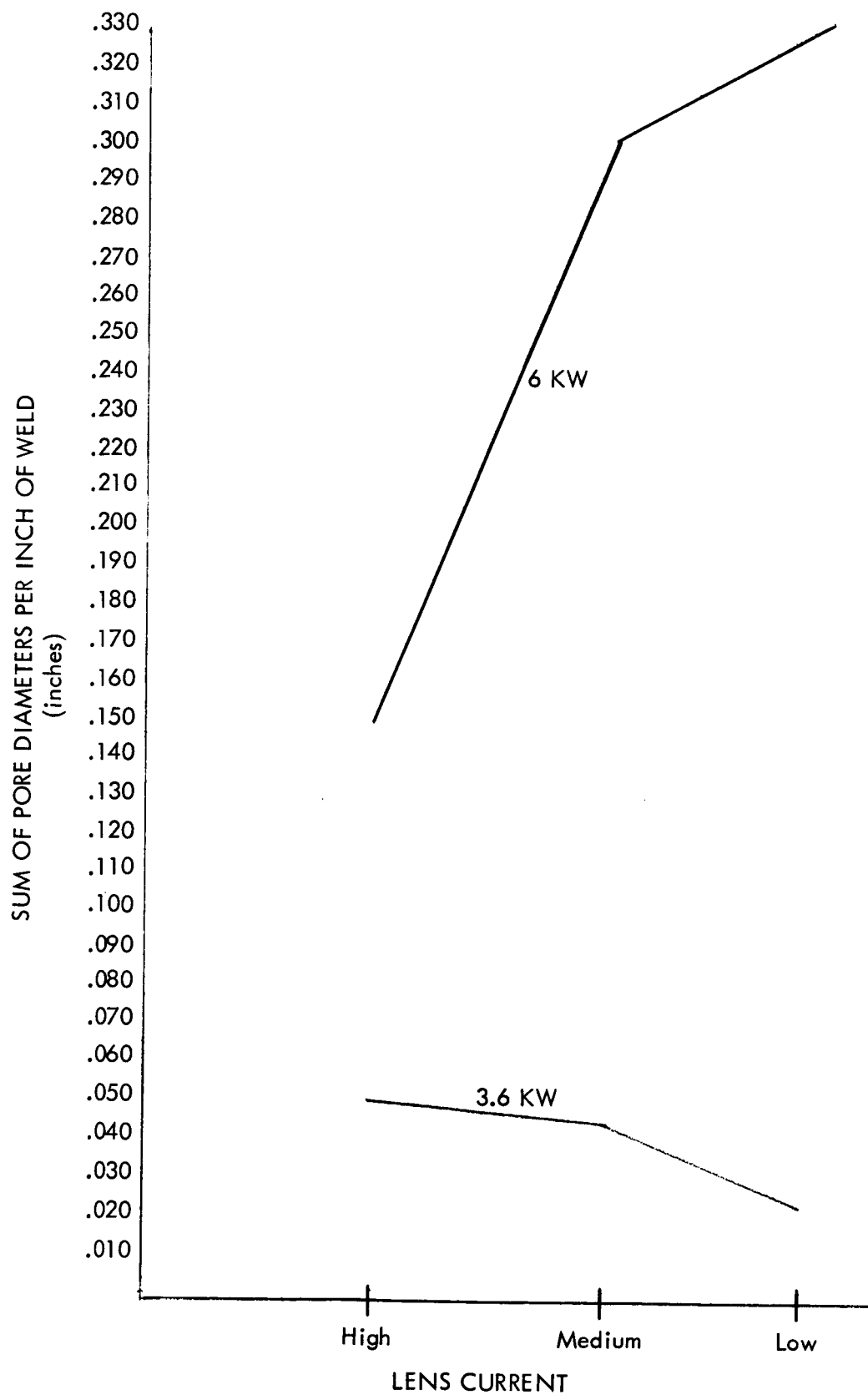
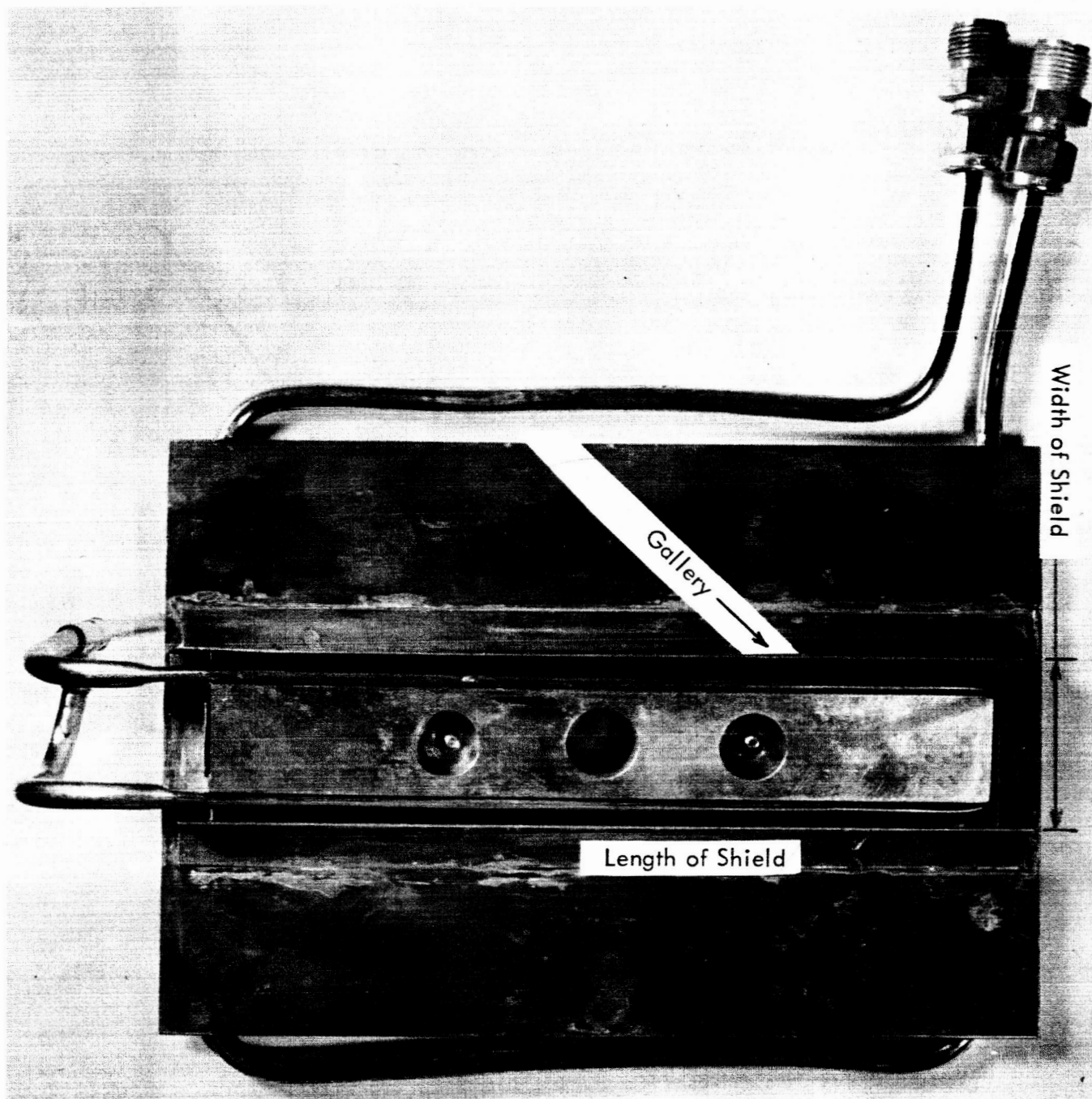
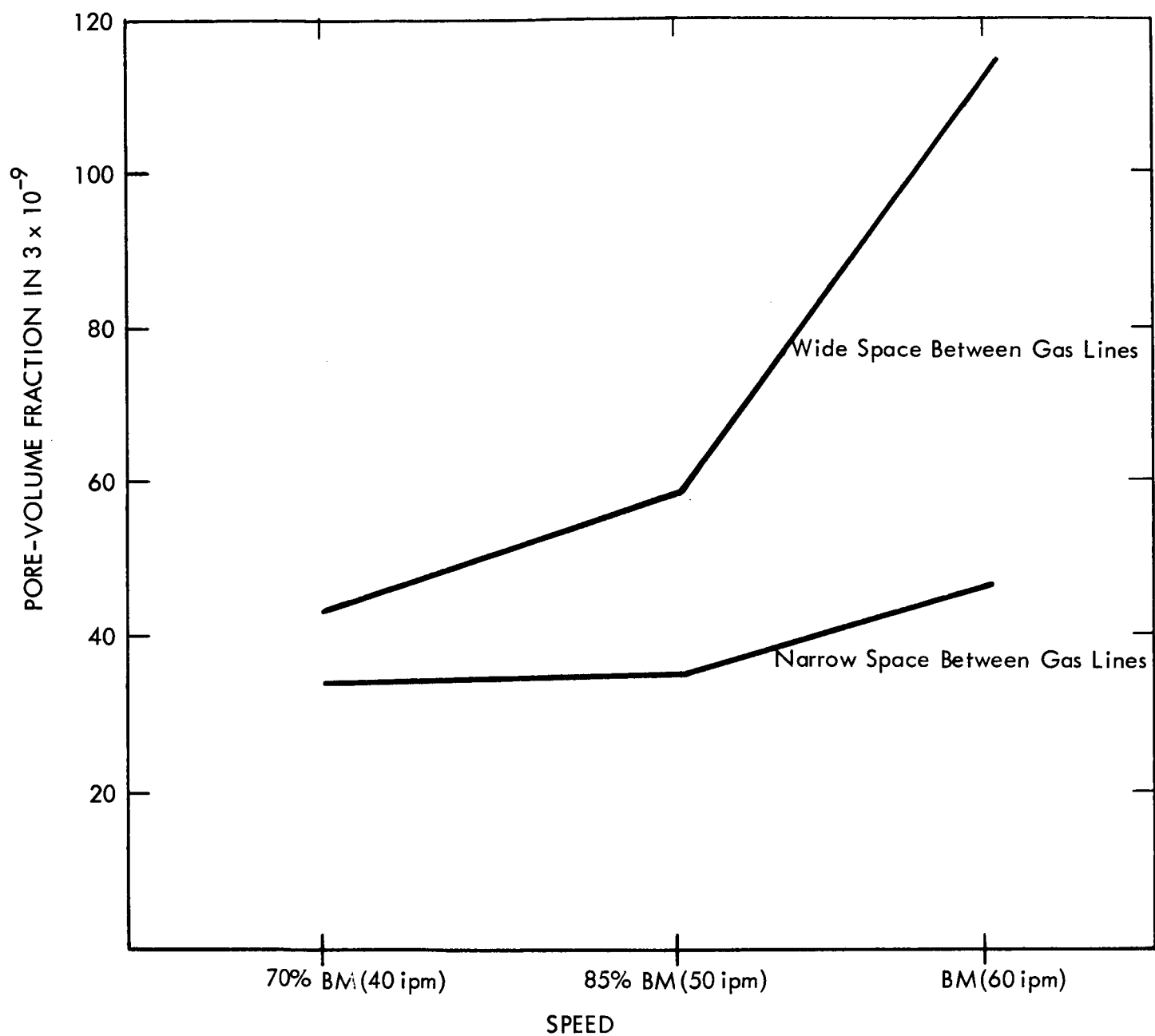


FIGURE 16
EFFECT OF LENS CURRENT ON POROSITY

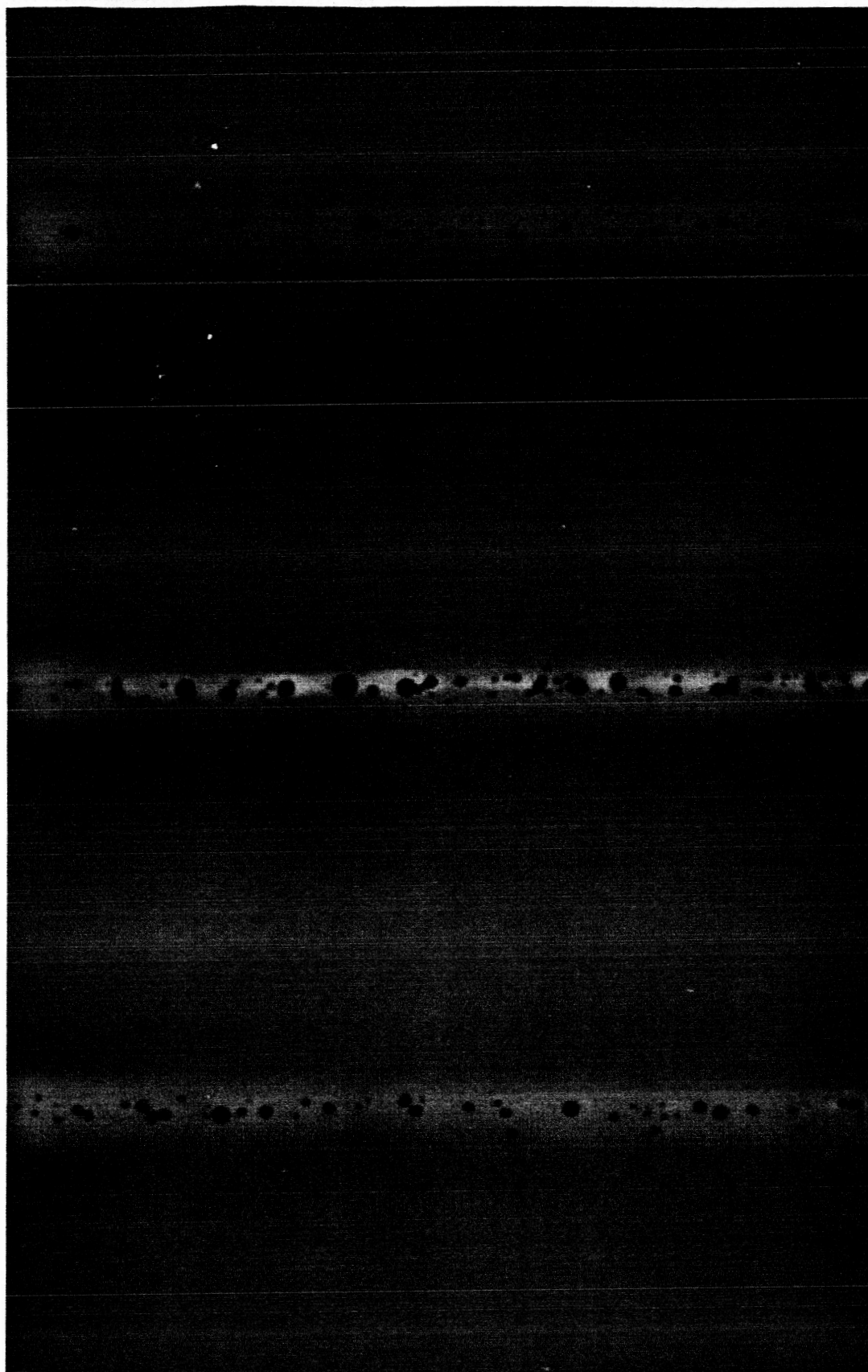


Assembled Gas Curtain Test Shield
(Bottom View)
Figure 17



FACTORS CAUSING CHANGE IN POROSITY LEVEL FOR A 6 KW WELDING PROCESS

FIG. 18



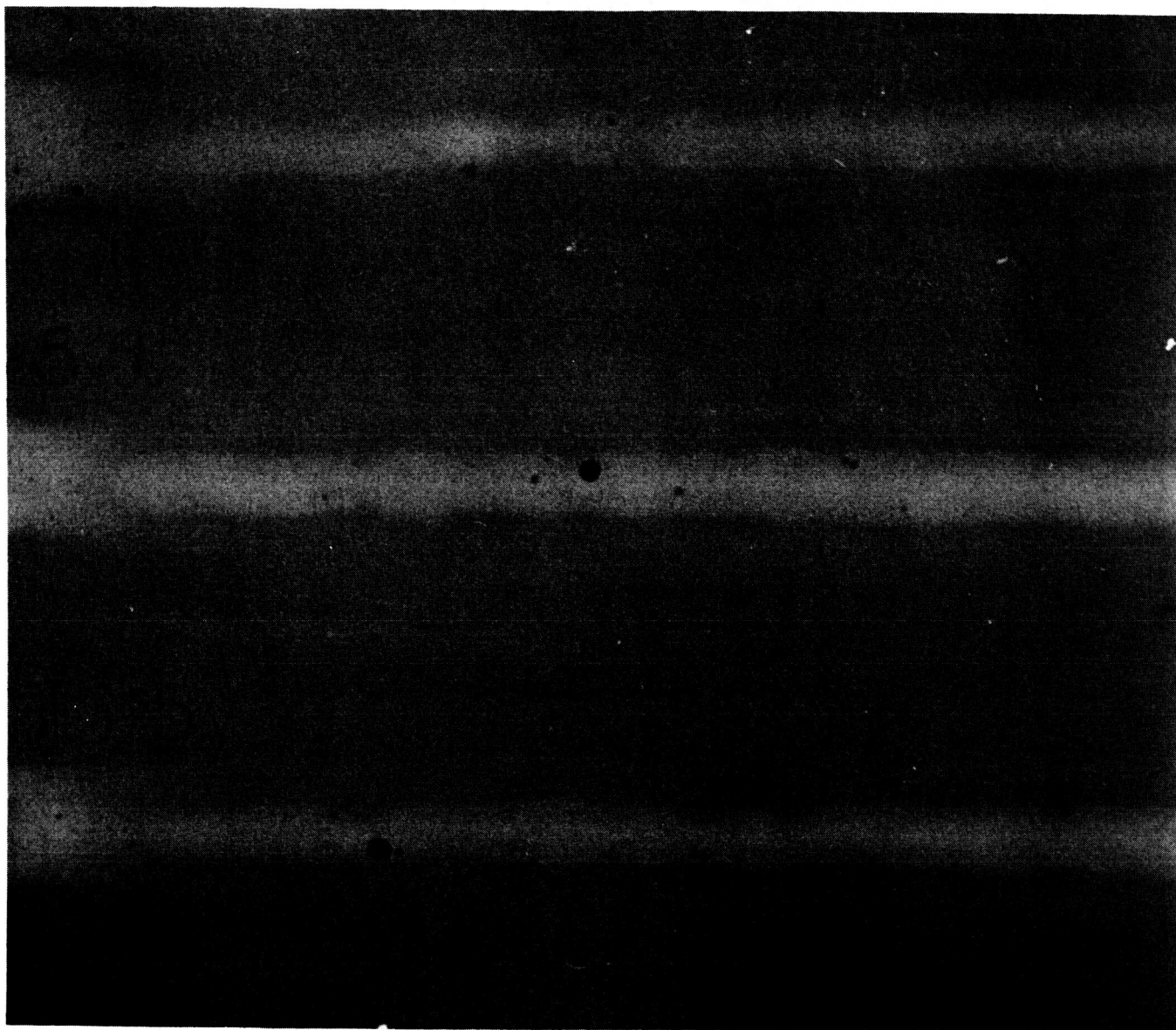
Radiograph Survey of Early Specimens with Non-Optimum Shielding and Cleaning Shows Severe Porosity for High Speed (60-70 ipm), High Power (6 KW) Procedure

2X

Top-to-Bottom; Short, Long, Medium Focus

Welds 88-90

FIGURE 19



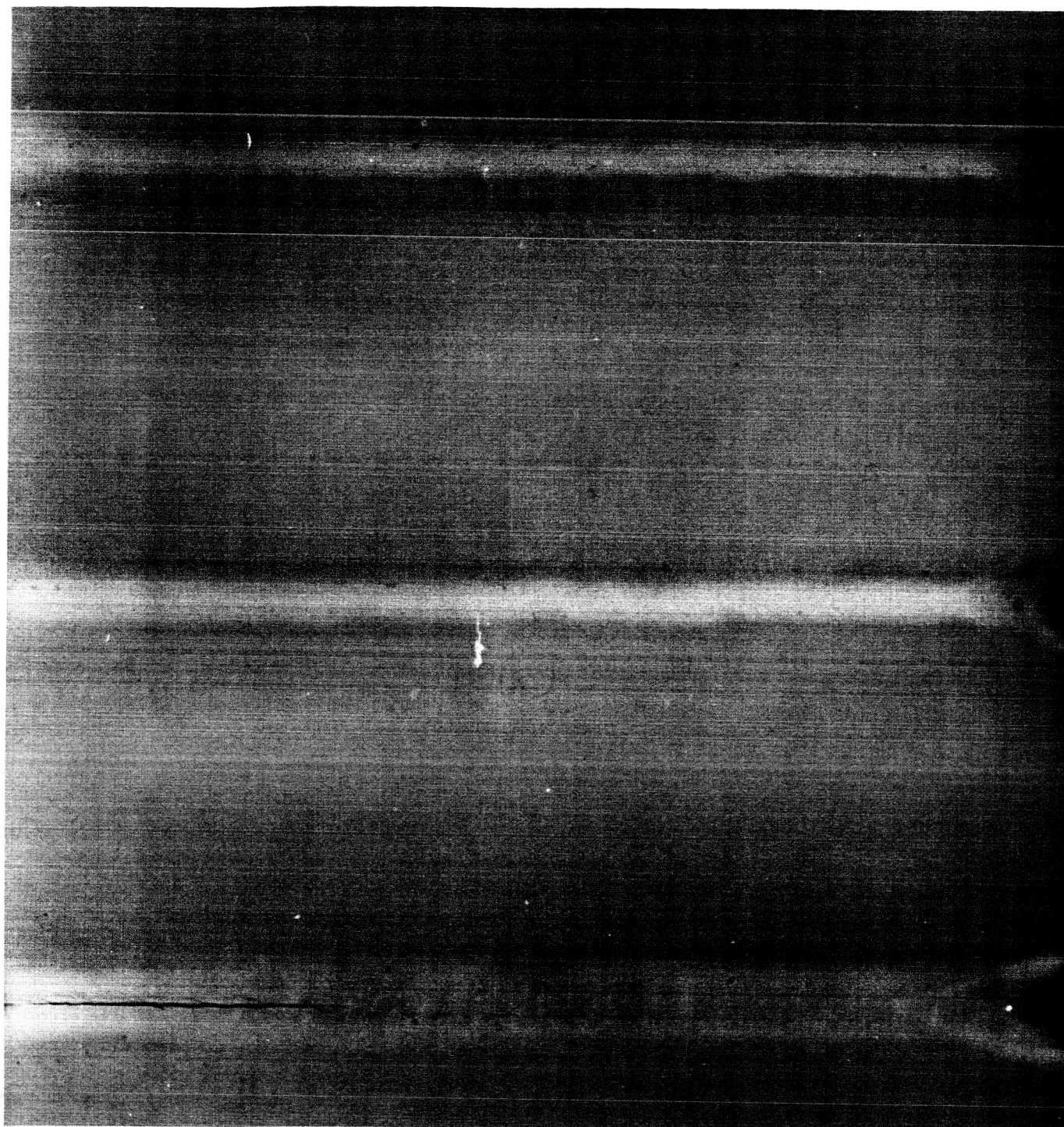
3.6 KW Procedure Produces Only Moderate Porosity In Spite of Non-Optimized Shielding
and Cleaning Practices

2.25X

Top-to-Bottom; Short, Long, Medium Focus

Welds 53-5

FIGURE 20



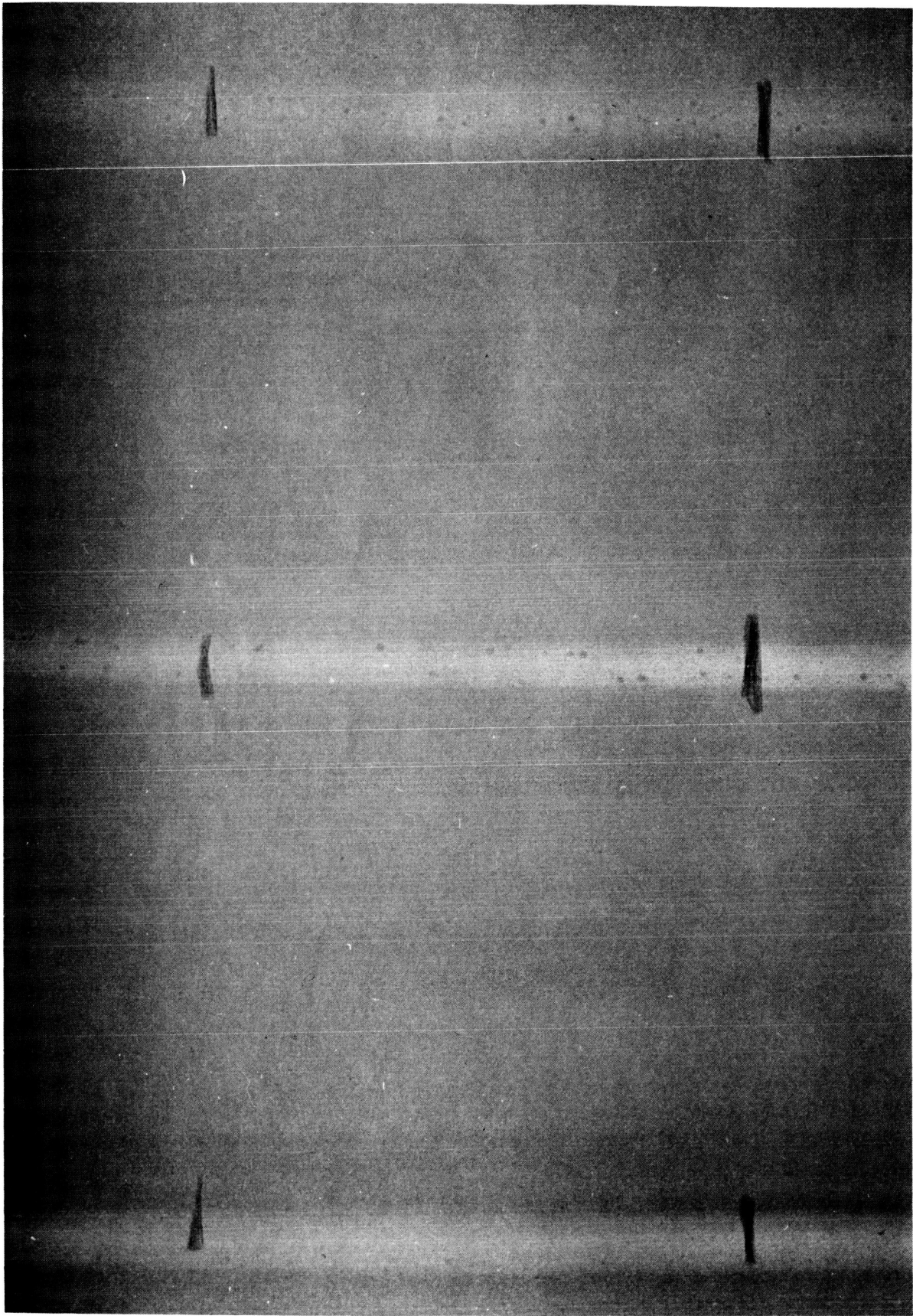
Optimum Shield Configuration (Closely Spaced Gas Manifolds) Reduces Porosity from 6 KW
Welding Procedure to Feasible Level

2X

Top-to-Bottom; 60 ipm (BM); 50 ipm; 40 ipm

Welds 166-8

FIGURE 21



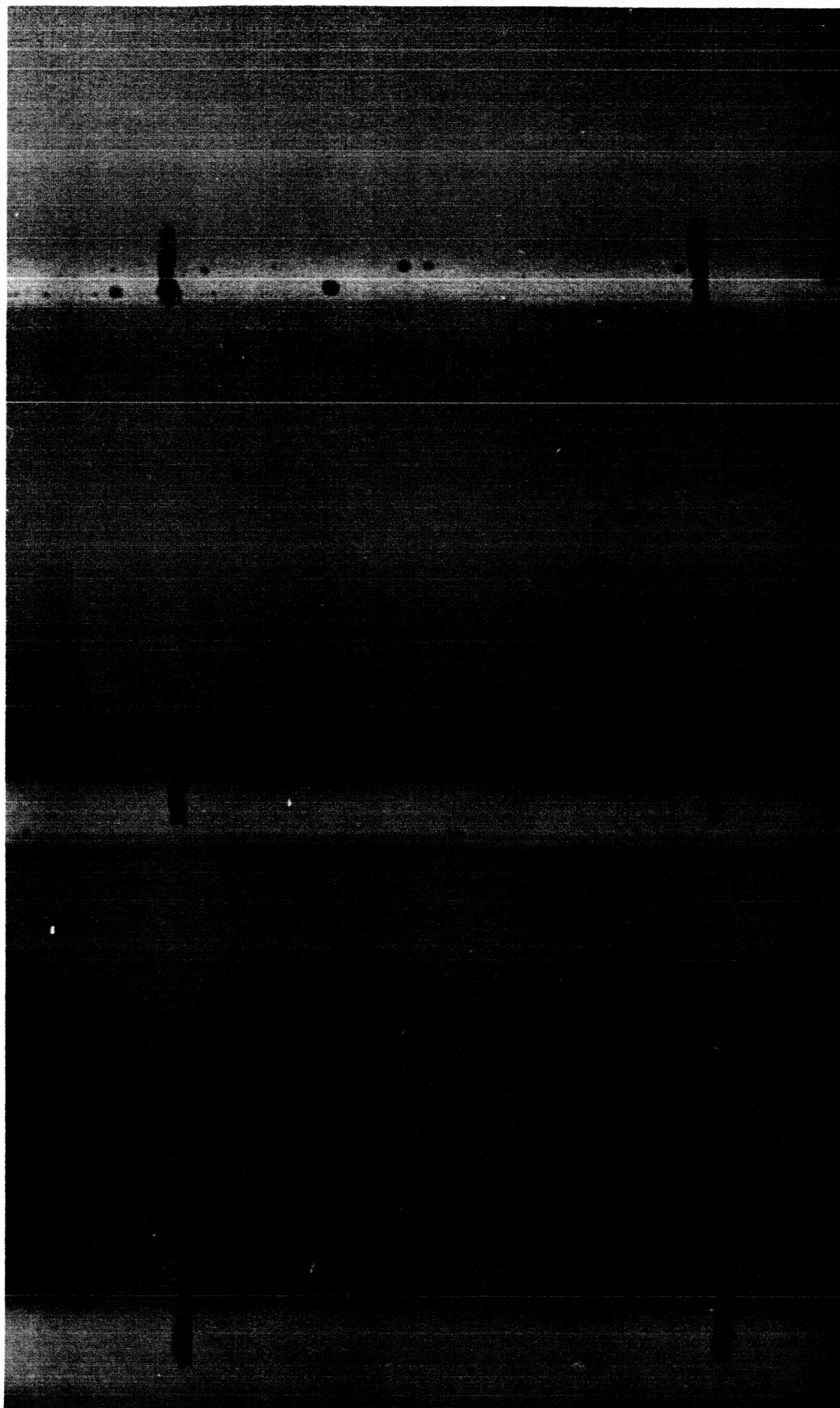
Porosity Level Obtained Using Shield Which Incorporates Both Diffuser and an Optimum Gas
Manifold Configuration

2X

Top-to-Bottom; 60 ipm (BM); 50 ipm; 40 ipm

Welds 254-6

FIGURE 22



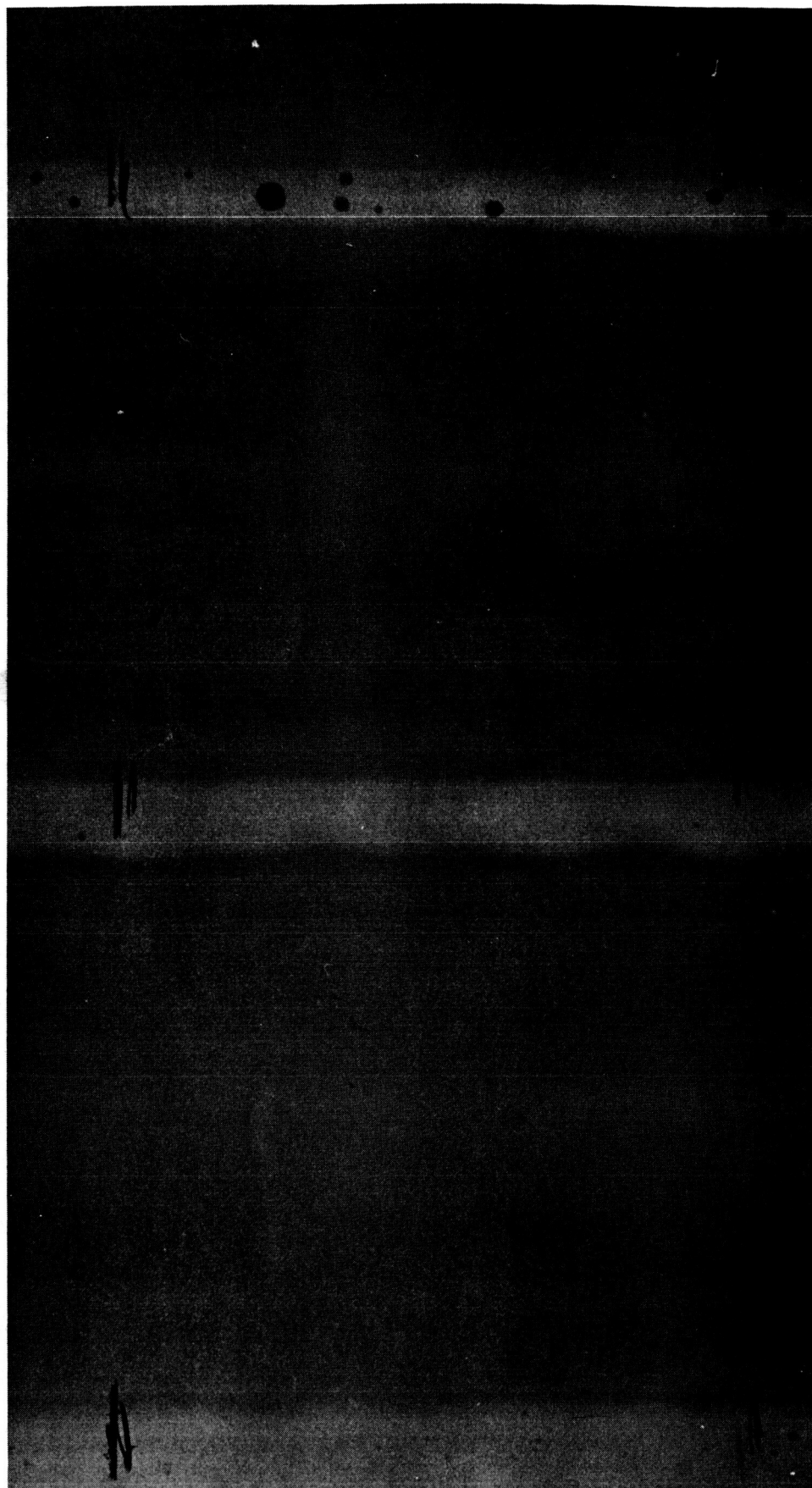
Porosity Level Obtained Using Optimized Shield, Diffuser and Chemical, (instead of Mechanical)
Cleaning Plus an Underbead Shield

2X

Top-to-Bottom; 60 ipm (BM); 50 ipm; 40 ipm

Welds 297-9

FIGURE 23



Porosity Level Obtained Using Optimized Shield Diffuser, Mechanical Cleaning and Underbead Shielding

2X

Top-to-Bottom; 60 ipm (BM); 50 ipm; 40 ipm

Welds 273-5

FIGURE 24

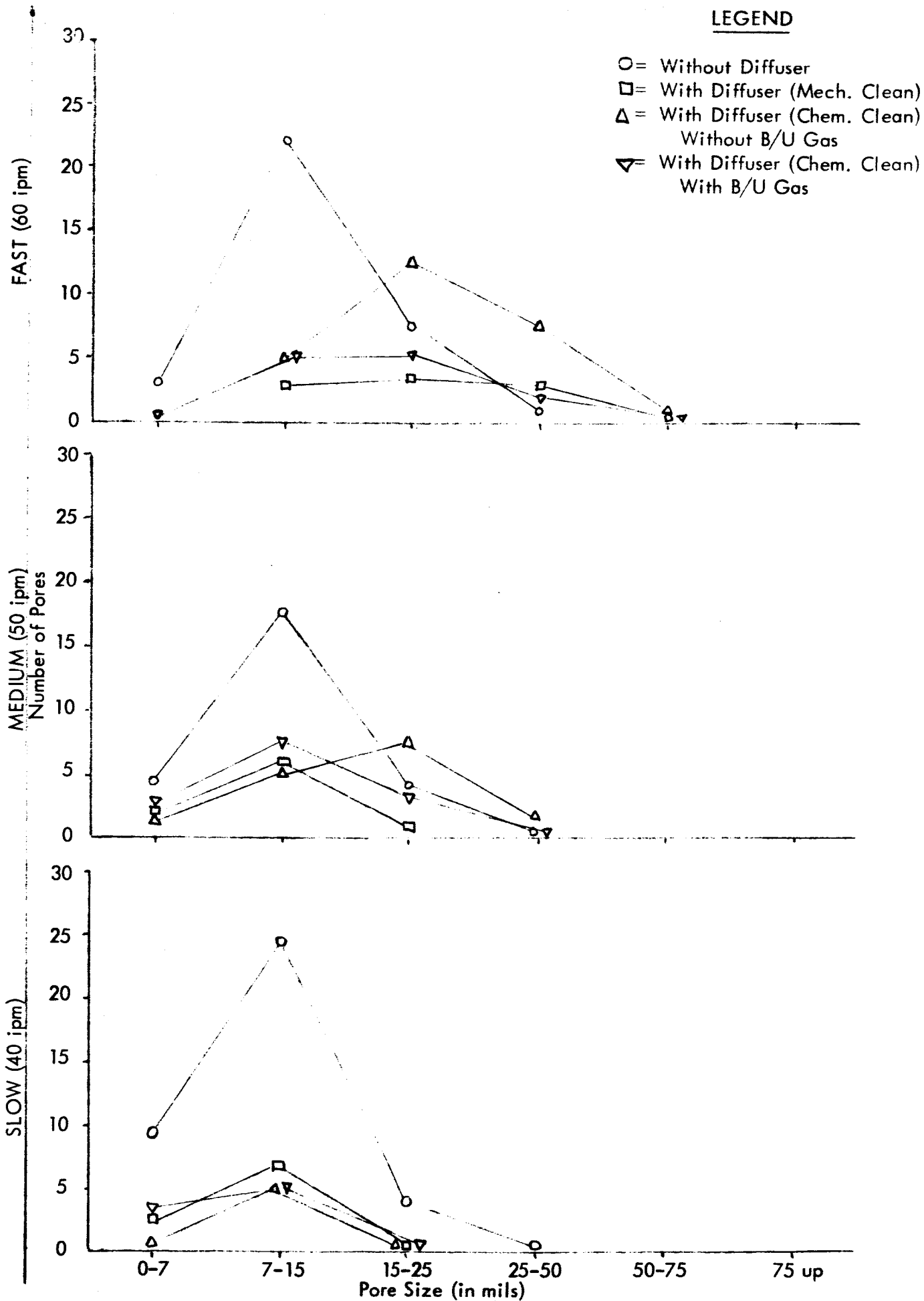


FIGURE 25 PORE SIZE & DISTRIBUTION AS FUNCTION OF TYPE OF CLEANING & DIFFUSER USE

WESTINGHOUSE ELECTRIC CORPORATION

LEGEND

- ◁ = One-Side, One-Pass
- S = Shaved Contour (Underhead Only)
- = Ⓢ 140 KV
- = Ⓢ 110 KV

ULTIMATE TENSILE STRENGTH ($\times 1000$ psi)

47
46
45
44
43
42
41
40

Proposed Time-Temperature Relationship *

* Ref: "Minutes Aluminum Weld Symposium" (NASA-MSFC)
July 1964, page 153

B.M.

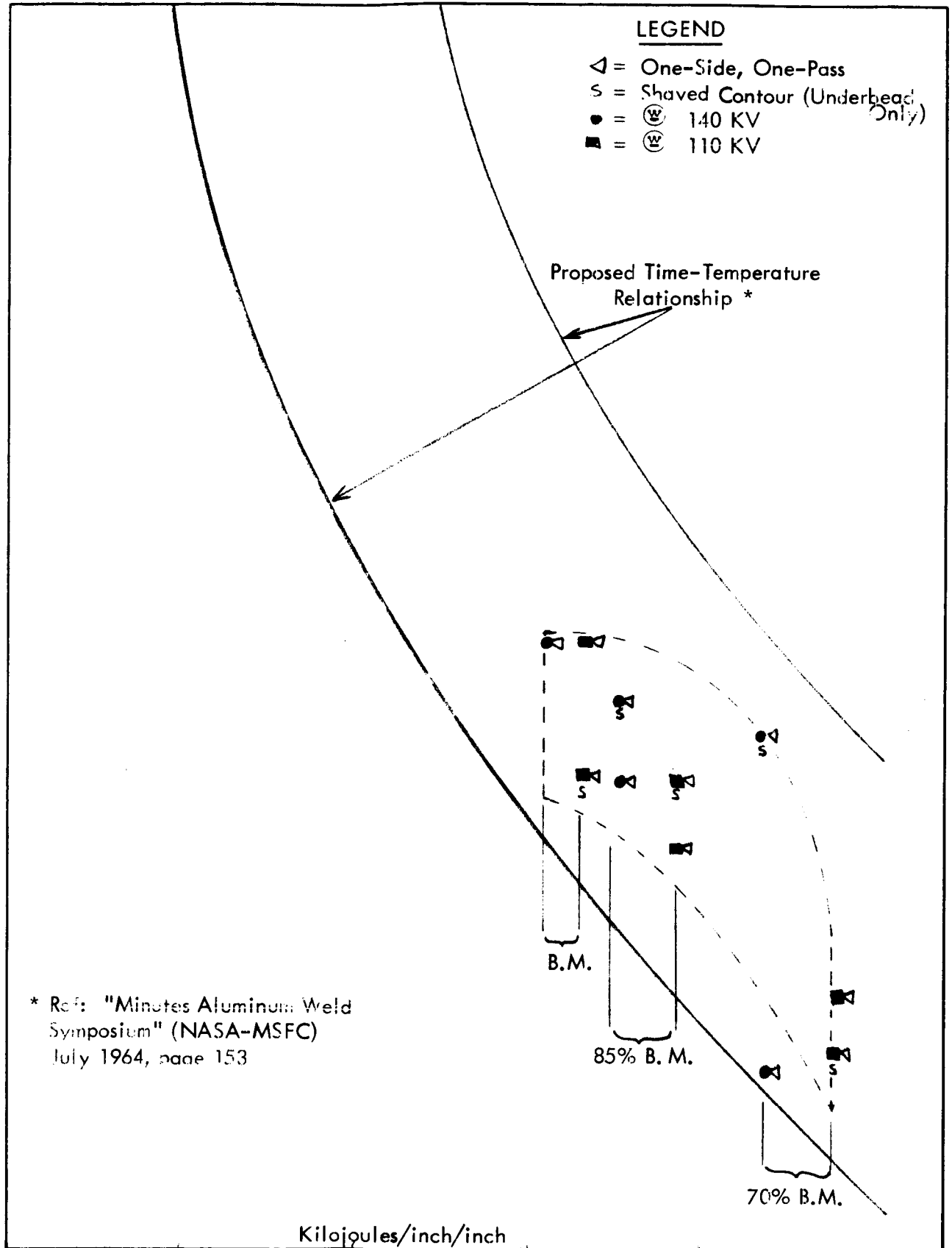
85% B.M.

70% B.M.

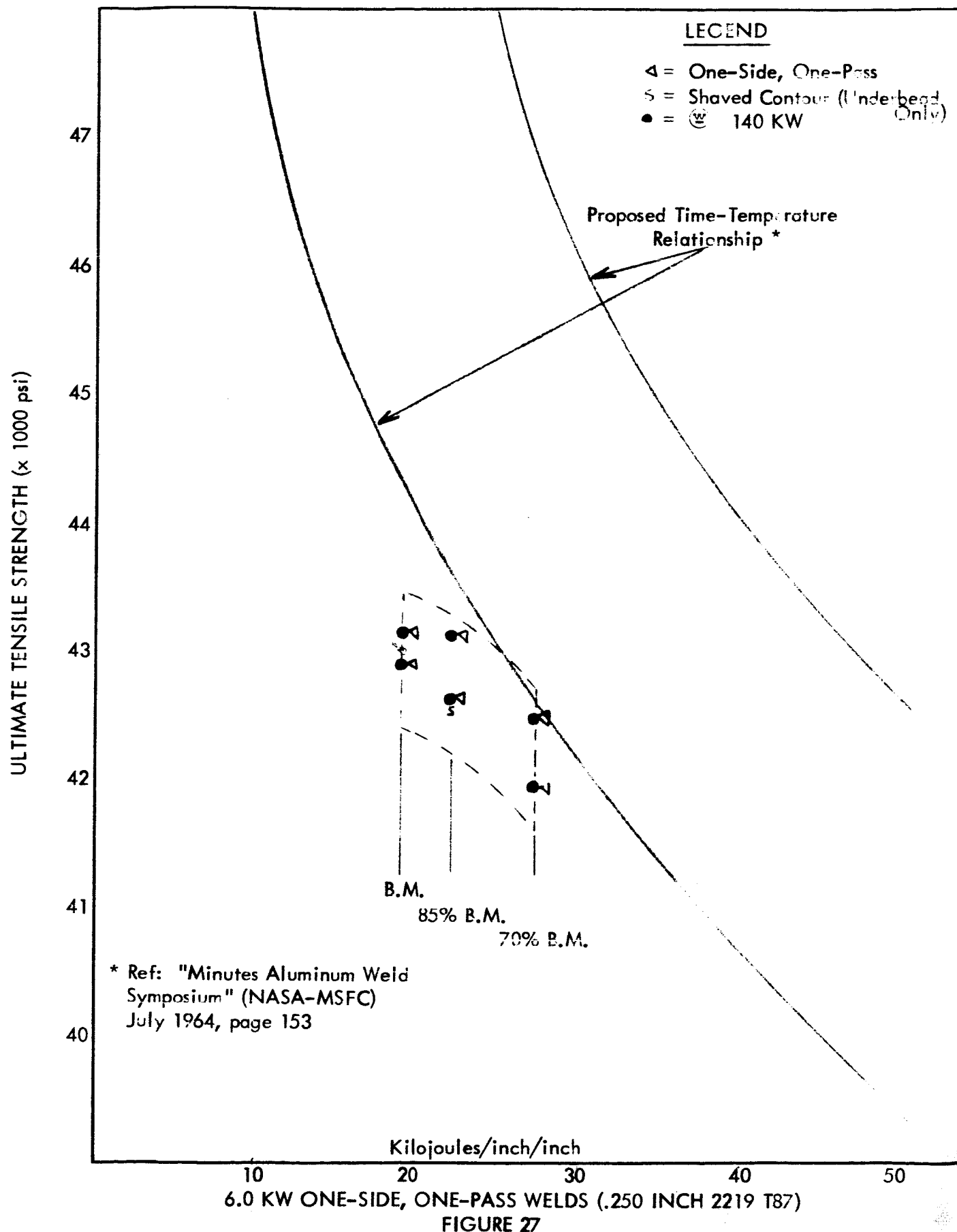
Kilojoules/inch/inch

3.6 KW ONE-SIDE, ONE-PASS WELDS (.250 INCH 2219 T87)

FIGURE 26



WESTINGHOUSE ELECTRIC CORPORATION



WESTINGHOUSE ELECTRIC CORPORATION

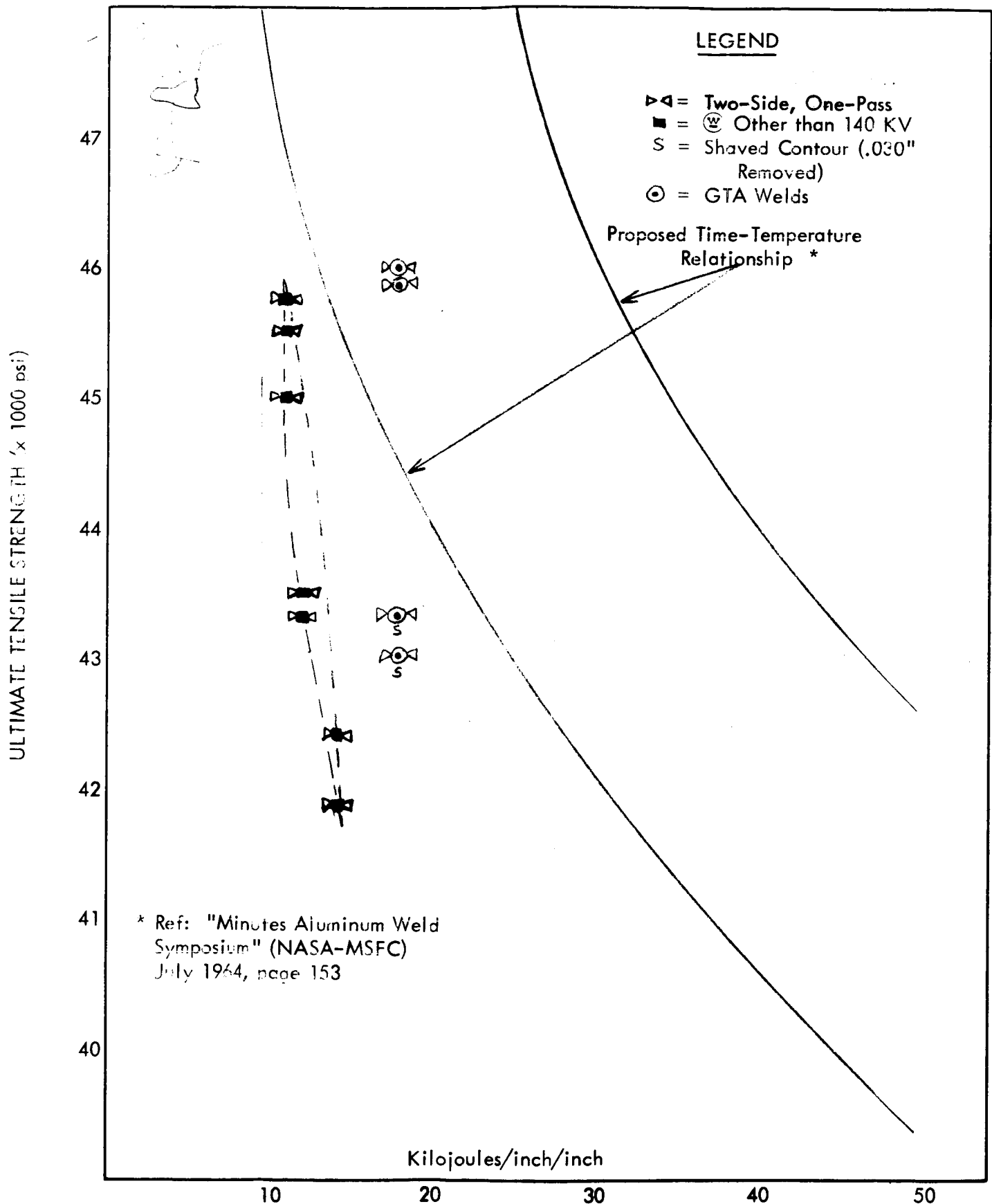


FIGURE 28 MINIMUM HEAT INPUT WELDS (120 ipm) TWO-SIDE, ONE-PASS WELDS (.250 INCH 2219 T87)

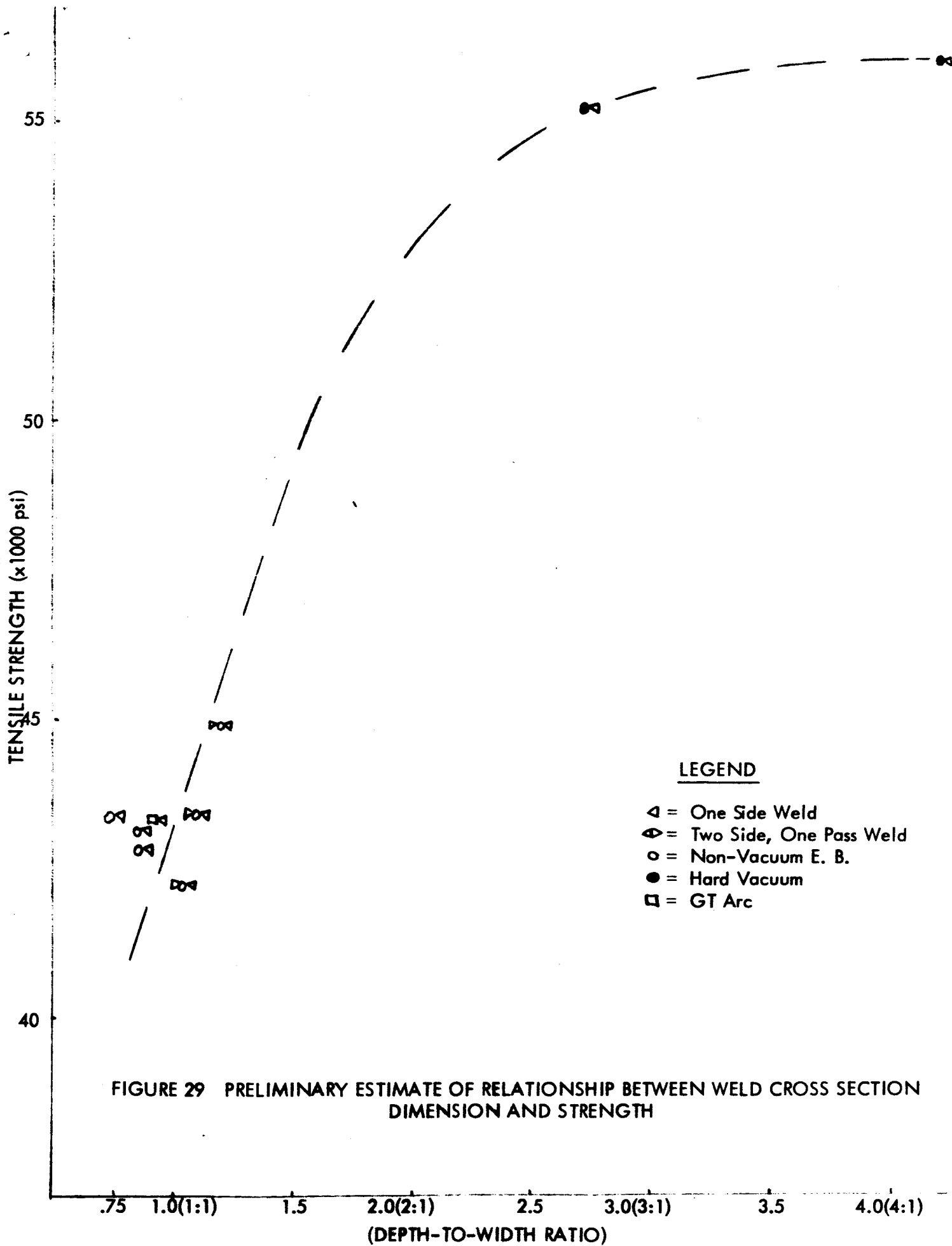


FIGURE 29 PRELIMINARY ESTIMATE OF RELATIONSHIP BETWEEN WELD CROSS SECTION DIMENSION AND STRENGTH

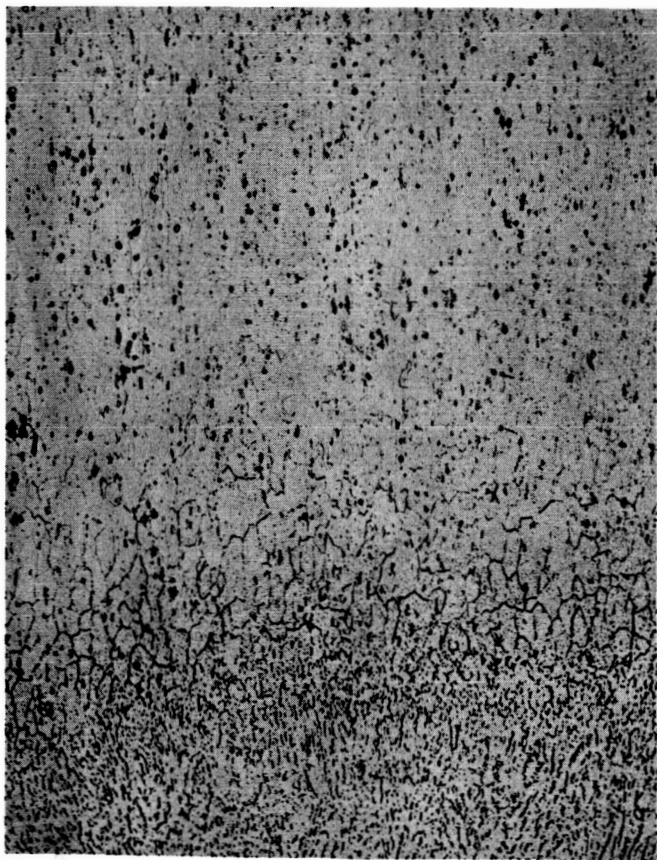


BASE

WELD 478-2
100X
Ksi = 45,000-45,760

HAZ

WELD



WELD 413-1
100X
Ksi = 40,000-42,000

HAZ

WELD

FIGURE 30. Structure and Extend of Heat Affected Zone of High and Low Strength Welds

26 OCT 65 74367
PROCESS POWER (KW)

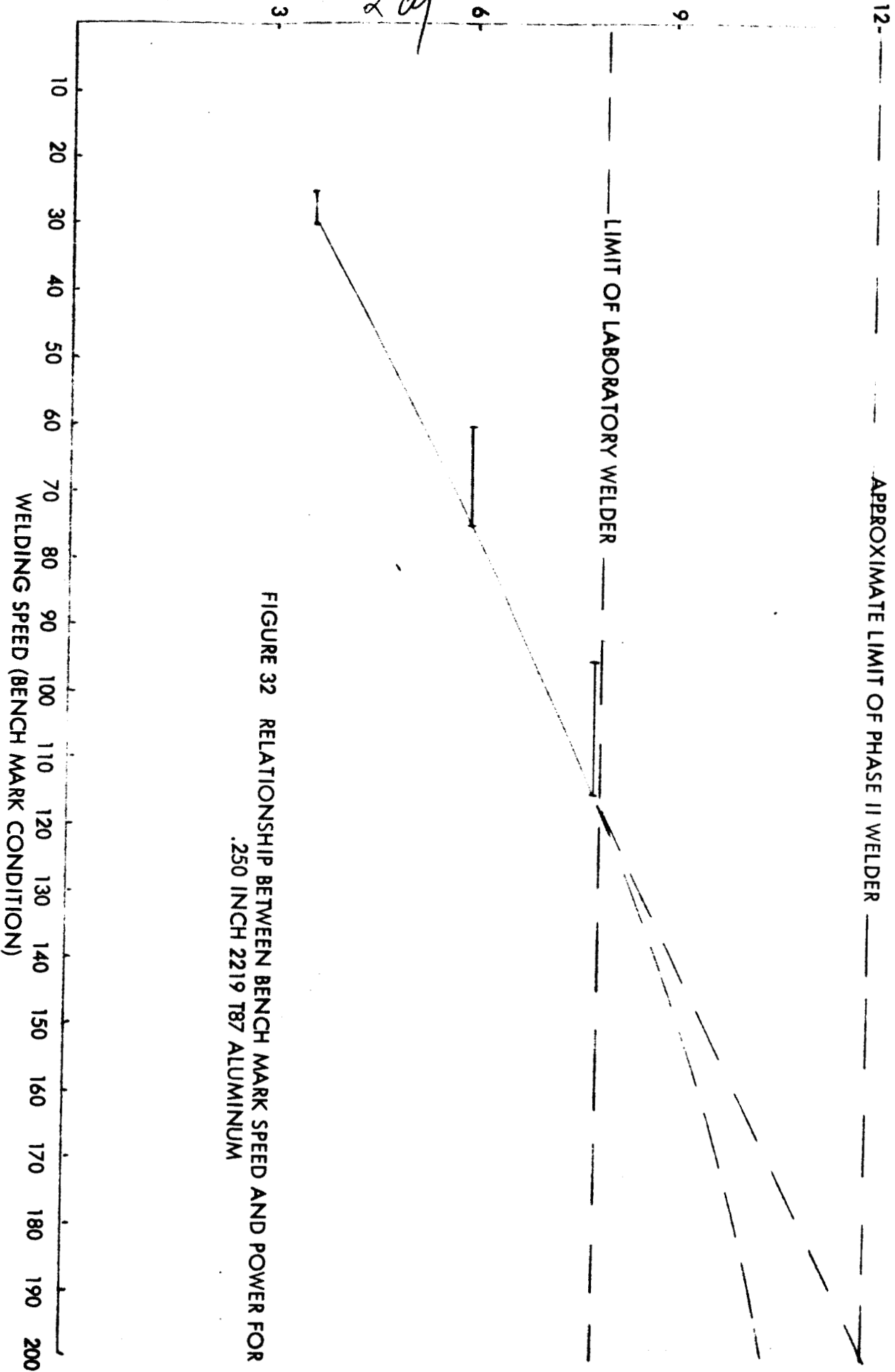


FIGURE 31 ESTIMATE OF RELATIONSHIP BETWEEN WELD WIDTH, PROCESS SPEED, AND WORKING DISTANCES FOR .250 2219 T87 ALUMINUM

